Article

Cyclometalated Platinum Complexes with Aggregation-Induced Phosphorescence Emission Behavior and Highly Efficient Electroluminescent Ability

Jiang Zhao, Zhao Feng, Daokun Zhong, Xiaolong Yang, Yong Wu, Guijiang Zhou, and Zhaoxin Wu

Chem. Mater., **Just Accepted Manuscript** • DOI: 10.1021/acs.chemmater.7b04708 • Publication Date (Web): 09 Jan 2018

Chemistry of Materials is published by the American Chemical Society. 1155 Sixteenth Street N.W., Washington, DC 20036

Cyclometalated Platinum Complexes with Aggregation-Induced Phosphorescence Emission Behavior and Highly Efficient Electroluminescent Ability

Jiang Zhao,[†] Zhao Feng,[†] Daokun Zhong,[†] Xiaolong Yang,[†] Yong Wu,[†] Guijiang Zhou,[*,†,¶] Zhaoxin Wu,[*,‡]

[†] MOE Key Laboratory for Nonequilibrium Synthesis and Modulation of Condensed Matter, Department of Chemistry, School of Science, Xi'an Jiaotong University, Xi'an 710049, P. R. China.

[¶] State Key Laboratory for Mechanical Behavior of Materials, Xi'an Jiaotong University, Xi'an 710049, P. R. China.

[‡] Key Laboratory of Photonics Technology for Information, School of Electronic and Information Engineering, Xi'an Jiaotong University, Xi'an, 710049, P. R. China

ABSTRACT

Aggregation-induced emission (AIE) materials can exhibit intense luminescence in aggregated or solid state, which are highly desirable for OLED application. However, only limited research results on developing AIE-active Pt^{II} complexes in electroluminescence (EL) application have been reported so far. Herein, a series of AIE-active Pt^{II}(C^N)(N-donor ligand)Cl complexes have been developed. Their chemical structures have been determined by NMR, MS and X-ray crystallography characterization. Theoretical results including the frontier molecular orbitals, the simulated UV-vis spectra and natural transition orbitals (NTO) have been employed to insightfully interpret their photophysical properties. It has also been found that much higher degree of molecular aggregation in these Pt^{II} complexes should be required to induce phosphorescent AIE than that for the fluorescent AIE behavior. These AIE-active Pt^{II} complexes can exhibit very strong emission in poly(methyl methacrylate) (PMMA) films with the phosphorescence quantum yield (Φ_p) of *ca.* 72.0%, while that in dilute solution is just about 4.7%. Accordingly, based on these AIE-active Pt^{II} complexes, the optimized OLEDs fabricated by the simple solution-processed strategy can achieve high EL efficiencies with a maximal external efficiency (η_{ext}) of 28.4%, a maximal current efficiency (η_L) of 75.9 cd A^{-1} and a maximal power efficiency (η_P) of 62.7 lm W^{-1}. Considering the rarity for EL investigations of the AIE-active Pt^{II} complexes, the concerned results realized by these Pt^{II}(C^N)(N-donor ligand)Cl complexes should provide valuable clues for exploring AIE-active Pt^{II} phosphorescent complexes with high EL performance.

INTRODUCTION

Organic light-emitting diodes (OLEDs) have obtained sustainable research interest both from academic and industrial researchers considering their promising application in flat panel displays and solid-state lighting sources.[1-4] Organometallic platinum complexes are one of the most promising candidates as phosphor materials within the OLEDs' emission layer (EML) for their attractive features such as high phosphorescent quantum yield (Φ_p), relatively short triplet state lifetime (τ_p) and tunable emission color.[5-9] Platinum complexes can harvest both the singlet and triplet excitons for light emission since the efficient intersystem crossing process induced by the strong spin-orbit coupling effect of the platinum atom. Hence, the maximal internal quantum efficiency (IQE) of phosphorescent emitters can reach 100%, leading to substantial improvement of their electroluminescent (EL) efficiency.[10, 11] According to the d^8 system of the Pt^{II} atom, it can be coordinated with various organic ligands to achieve the preferred coordination number 4 with a spuare planar geometry. Recently, different organic ligands including 1,3-bis(2-pyridyl)benzene (N^C^N),[12, 13] 6-phenyl-2,2'-bipyridine (N^N^C),[14, 15] 2,6-diphenylpridine (C^N^C)[16]and 2-phenylpyridine(C^N, ppy)[7, 17, 18] as well as their derivatives have been adopted to synthesize platinum complexes. Among these platinum complexes, ppy-type platinum complexes in presence of one β-diketonato ancillary ligand (Pt^{II}(C^N)acac) have been extensively developed for OLED applications due to their tunable photoelectric properties by using different peripheral substituent groups.[7, 19] Similar to the fluorescent materials, the emission of some ppy-type cyclometalated Pt^{II} complexes can be quenched in high concentration solution or aggregation state, known as aggregation-caused quenching effect (ACQ), which immensely hinders their application in OLED field.[20-22] Hence, efforts have to be devoted to bypass this obstacle for improving EL performance of

Pt^{II} complexes.

In 2001, Tang *et al* discovered the very different light-emitting behaviors of some silole derivatives in solution and solid states. Weak or non-emissive in dilute solution but highly luminescent when their molecules aggregate in concentrated solutions or solid state, which has been defined as aggregation-induced emission (AIE).[23-25] This discovery offers exciting inspirations to design and synthesize Pt^{II} complexes with high EL performance, changing the emission behavior from ACQ to AIE.[26-28] To date, some Pt^{II} complexes with AIE character have been reported.[21, 29-32] Huang's group has established a series of ppy-type AIE-active Pt^{II} complexes for bioimaging applications.[33] Liu *et al* reported a series of Pt^{II} diimine acetylide complexes with good AIE nature and optical power limiting property.[34] Yam's group developed two unsymmetric bipyridine–Pt^{II}–alkynyl complexes with AIE nature, which have been employed in OLED application showing maximal η_L of 18.4 cd A^{-1} and η_{ext} of 5.8%.[35] After replacing the β-diketonato ancillary ligand of Pt^{II}(C^N)acac with one chloride and N-donor ligand, AIE-active heteroleptic Pt^{II}(C^N)(N-donor ligand)Cl complexes can be obtained[26, 27], which have been employed to investigate their structural features,[36] biological activity[26, 37, 38] and catalytic performance,[39] *etc*. To the best of our knowledge, the EL studies of the Pt^{II} complexes with AIE character are still of shortage. Therefore, the exploring of AIE-active Pt^{II} complexes for EL application can be significantly meaningful. Similar to the Pt^{II}(C^N)acac complexes, the photoelectric properties of the Pt^{II}(C^N)(N-donor ligand)Cl complexes can be readily tunable by manipulating the C^N and N-donor ligands, showing a good potential in EL field. However, apart from two complexes with good EL performance developed by our group[40] and two complexes with a maximal η_L of 0.5 cd A^{-1} [41], studies on the EL properties of the Pt^{II}(C^N)(N-donor ligand)Cl complexes are very sparse. Hence,

it is very worthwhile to study the EL properties of this class of AIE-active Pt^{II}(C^N)(N-donor ligand)Cl complexes. Given the significant influence of charge balance between electrons and holes from opposite electrodes on OLEDs' performance, it is highly desirable that Pt^{II} complexes can exhibit good charge carrier injection/transporting features.[42-44] Considerable research efforts have been devoted by Zhou *et al* to describe that Ir^{III} and Pt^{II} complexes can achieve efficient EL performance by chelating with functionalized ppy-type ligands bearing $–NPh_2$, $–POPh_2$ and $–SO_2Ph$ moieties showing more balanced charge carrier injection/transporting abilities.[7, 42, 45-47] Hence, the introduction of these functional moieties into the AIE-active Pt^{II} complexes should be advisable for their EL improvement.

Herein, four AIE-active heteroleptic Pt^{II}(C^N)(N-donor ligand)Cl type complexes are presented, their preparation, thermal stability, electrochemistry and photophysical properties have been investigated in detail and were corroborated by theoretical calculations. The OLEDs as well as single carrier devices based on the concerned Pt^{II} complexes are fabricated by solution process and their EL properties are studied. The AIE property and balanced charge carrier injection/transporting ability of the concerned Pt^{II} complexes should be significantly beneficial for the EL enhancement. This research should offer critical clues for developing novel phosphorescent Pt^{II} complexes with AIE nature and promoting their application in EL field.

EXPERIMENTAL SECTION

General Information. Under nitrogen atmosphere, all reactions were carried out with the use of standard Schlenk techniques. The solvents were purified by standard methods under dry nitrogen before use. All commercially available reagents were used as received unless otherwise stated. The

reactions were monitored by thin-layer chromatography (TLC) with Merck pre-coated aluminum plates. Flash column chromatography and preparative TLC were carried out using silica gel. The detailed information for the physical characterization, X-ray crystallography, theoretical calculation and OLED fabrication and measurements are provided in the Supplementary Information (SI).

Synthesis. Preparation details of the cyclometalating ppy-type ligands **L-N**, **L-P** and **L-S** were according to the reported literature.[7] The synthesis details for some related compounds are presented in the Supplementary Information (SI).

General Procedures for the Synthesis of N-donor Ligands: Under a N_2 atmosphere, 4-bromopyridine hydrochloride (1.0 equiv), the corresponding borate compound or boronic acid (1.2 equiv, Scheme S1), and $Pd(PPh_3)_4$ (5 mol-%) were heated to 110 ^oC in a mixture of 10 mL 2M Na_2CO_3 and 25 mL degassed THF for 24 h. After cooling to room temperature, the mixture was extracted with dichloromethane, the organic phase was dried over Na_2SO_4 and the solvent was removed under reduced pressure. The residue was obtained as a crude product, which was chromatographed on a silica column to produce a pure product.

N-4-N: (Yield: 62%); ^1H NMR (400 MHz, $CDCl_3$, δ): 8.62 (d, *J* = 6.40 Hz, 2 H), 7.52 (d, *J* = 8.80 Hz, 4 H), 7.30 (t, *J* = 8.40 Hz, 4 H), 7.15–7.13 (m, 6 H), 7.8 (t, *J* = 7.20 Hz, 2 H); ^{13}C NMR (100 MHz, $CDCl_3$, δ): 150.16, 148.92, 147.63, 147.22, 130.91, 129.41, 127.61, 124.96, 123.58, 122.89, 120.86; FAB-MS (*m/z*): 322 $[M]^+$; Elemental analysis calcd (%) for $C_{23}H_{18}N_2$: C 85.68, H 5.63, N 8.69; found: C 85.57, H 5.55, N 8.58.

N-4-S: (Yield: 68%); ^1H NMR (400 MHz, $CDCl_3$, δ): 8.71 (d, *J* = 1.60 Hz, 2 H), 8.08-8.05 (m, 2 H), 8.01-7.98 (m, 2 H), 7.76–7.74 (m, 2 H), 7.62-7.58 (m, 1 H), 7.57-7.52 (m, 2 H), 7.48-7.46 (m, 2 H); ^{13}C NMR (100 MHz, $CDCl_3$, δ): 150.55, 146,37, 143.06, 142.00, 141.29, 133.41, 129.40, 128.46,

127.97, 127.72, 121.72; FAB-MS (*m/z*): 295 $[M]^+$; Elemental analysis calcd (%) for $C_{17}H_{13}NO_2S$: C 69.13, H 4.44, N 4.74; found: C 69.05, H 4.39, N 4.68.

N-4-P: (Yield: 52%); ^{1}H NMR (400 MHz, $CDCl_3$, δ): 8.70 (d, *J* = 5.60 Hz, 2 H), 7.82-7.77 (m, 2 H), 7.73-7.68(m, 6 H), 7.57 (t, *J* = 7.60 Hz, 2 H), 7.51-7.47 (m, 6 H); ^{31}P NMR (162 MHz, $CDCl_3$, δ) 28.65; ^{13}C NMR (100 MHz, $CDCl_3$, δ): 150.42, 147,06, 141.58, 133.87, 132.89, 132.65, 132.12, 131.96, 128.64, 127.13, 121.65; FAB-MS (*m/z*): 355 $[M]^+$; Elemental analysis calcd (%) for $C_{23}H_{18}NOP$: C 77.74, H 5.11, N 3.94; found: C 77.62, H 4.95, N 3.86.

General Procedures for the Synthesis of Pt^{II} Complexes: Under a N_2 atmosphere, the organic cyclometalating ligands (**L-N**, **L-P** and **L-S**, 1.1 equiv) and K_2PtCl_4 (1 equiv) were heated to 90 ^oC and stirred for 18 h in 15 mL mixture of H_2O and 2-ethoxyethanol (v/v = 1 : 3). Then the reaction mixture was cooled to room temperature, and water was added. The precipitate of μ-chloro-bridged dimer was collected and dried under vacuum. Without further purification, the dimer and N-donor ligands (**N-4-N**, **N-4-P** and **N-4-S**) were added in 10 ml chloroform and heated to 50 ^oC for 12 h. After cooling to room temperature, the mixture was extracted with dichloromethane. The organic phase was dried over anhydrous Na_2SO_4 and the solvent was removed under reduced pressure. The residual was purified by flash column chromatography using appropriate eluent.

N-Pt-P: yellow solid (Yield: 79%). ^{1}H NMR (400 MHz, $CDCl_3$, δ): 9.59 (d, *J* = 5.60 Hz, 1H), 8.83 (d, *J* = 6.40 Hz, 2H), 7.86 (d, *J* = 8.40 Hz, 1H), 7.84 (d, *J* = 8.00 Hz, 1H), 7.77–7.70 (m, 5H), 7.64–7.59 (m, 4H), 7.54–7.50 (m, 5H), 7.33–7.27 (m, 3H), 7.17 (t, *J* = 7.60 Hz, 4H), 7.04 (d, *J* = 7.60 Hz, 5H), 6.92 (t, *J* = 7.20 Hz, 2H), 6.80 (dd, *J* = 2.40, 8.4 Hz, 1H), 5.93 (d, *J* = 2.00 Hz, 1H); ^{13}C NMR (100 MHz, $CDCl_3$, δ): 166.81, 153.91, 151.11, 149.38, 148.37, 147.17, 142.26, 139.63, 138.61, 137.76, 135.33, 134.31, 133.06, 132.96, 132.09, 131.99, 131.40, 129.11, 128.77, 128.65,

127.12, 127.00, 125.44, 124.55, 123.85, 123.51, 120.58, 117.56, 116.80; ^{31}P NMR (162 MHz, $CDCl_3$, δ): 28.35; FAB-MS (*m/z*): 930.1572 $[M+Na]^+$, 871.2030 $[M–Cl]^+$; Elemental analysis calcd (%) for $C_{46}H_{35}ClN_3OPPt$: C 60.89, H 3.89, N 4.63; found: C 60.81, H 3.79, N 4.56.

N-Pt-S: yellow solid (Yield: 76%). ^{1}H NMR (400 MHz, $CDCl_3$, δ): 9.58 (d, *J* = 6.00 Hz, 1H), 8.85 (d, *J* = 6.80 Hz, 2 H), 8.10 (d, *J* = 8.4 Hz, 2 H), 8.01 (d, *J* = 7.60 Hz, 2 H), 7.75 (t, *J* = 7.2 Hz, 1 H), 7.65–7.61 (m, 3 H), 7.56 (t, *J* = 7.60 Hz, 2 H), 7.50 (d, *J* = 8.00 Hz, 1 H), 7.32 (d, *J* = 2.20, 1 H), 7.24 (d, *J* = 6.80 Hz, 2 H), 7.17 (t, *J* = 4.00 Hz, 4 H), 7.05 (t, *J* = 6.80 Hz, 5 H), 6.91 (t, *J* = 7.20 Hz, 2 H), 6.80 (dd, *J* = 2.00, 4.20 Hz, 1 H), 5.91 (d, *J* = 2.00 Hz, 1 H); ^{13}C NMR (100 MHz, $CDCl_3$, δ): 166.75, 154.04, 151.09, 149.33, 147.57, 147.15, 143.03, 142.17, 140.99, 140.96, 138.68, 137.75, 133.64, 129.51, 129.10, 128.61, 127.96, 127.80, 125.44, 124.58, 123.75, 123.59, 123.33, 120.62, 117.59, 116.85; FAB-MS (*m/z*): 873.1991 $[M+Na]^+$, 811.1591 $[M–Cl]^+$; Elemental analysis calcd (%) for $C_{40}H_{30}ClN_3O_2PtS$: C 56.70, H 3.57, N 4.96; found: C 56.59, H 3.61, N 4.85.

P-Pt-N: yellowish green solid (Yield: 72%). ^{1}H NMR (400 MHz, $CDCl_3$, δ): 9.75 (d, *J* = 5.20 Hz, 1 H), 8.65 (d, *J* = 6.80 Hz, 2 H), 7.88 (t, *J* = 4.00 Hz, 1 H), 7.73 (d, *J* = 8.00 Hz, 1 H), 7.58–7.53 (m, 6 H), 7.50 (d, *J* = 8.80 Hz, 2 H), 7.38–7.28 (m, 11 H), 7.24–7.12 (m, 10 H), 6.57 (d, *J* = 12.40 Hz, 1 H); ^{13}C NMR (100 MHz, $CDCl_3$, δ): 166.06, 153.05, 151.73, 150.20, 149.03, 148.25, 146.70, 139.05, 138.61, 134.26, 134.16, 133.15, 133.00, 132.04, 131.94, 129.62, 128.30, 127.70, 127.54, 127.46, 127.36, 125.60, 124.34, 123.28, 123.15, 123.00, 122.14, 121.67, 119.06; ^{31}P NMR (162 MHz, $CDCl_3$, δ): 29.43; FAB-MS (*m/z*): 930.1569 $[M+Na]^+$, 871.2015 $[M–Cl]^+$; Elemental analysis calcd (%) for $C_{46}H_{35}ClN_3OPPt$: C 60.89, H 3.89, N 4.63; found: C 60.78, H 3.82, N 4.59.

S-Pt-N: yellowish green solid (Yield: 78%). ^{1}H NMR (400 MHz, $CDCl_3$, δ): 9.75 (d, *J* = 6.00 Hz, 1 H), 8.79 (d, *J* = 6.80 Hz, 2 H), 7.91–7.86 (m, 1 H), 7.77 (d, *J* = 8.00 Hz, 2 H), 7.75 (t, *J* = 7.20 Hz,

1 H), 7.71–7.66 (m, 2 H), 7.62 (d, J = 4.80 Hz, 2 H), 7.58 (d, J = 4.80 Hz, 2 H), 7.56–7.49 (m, 2 H), 7.41 (t, J = 8.00 Hz, 2 H), 7.34 (t, J = 7.60 Hz, 4 H), 7.27–7.12 (m, 8 H), 6.97 (d, J = 2.80 Hz, 1 H); ^{13}C NMR (100 MHz, $CDCl_3$, δ): 166.16, 153.32, 151.83, 150.31, 149.74, 149.42, 146.73, 143.07, 141.61, 141.43, 139.16, 133.02, 129.59, 129.07, 127.87, 127.61, 127.59, 125.56, 124.28, 123.61, 123.44, 122.53, 122.43, 121.91, 119.38; FAB-MS (*m/z*): 871.1681 $[M+Na]^+$, 811.1598 $[M–Cl]^+$; Elemental analysis calcd (%) for $C_{40}H_{30}ClN_3O_2PtS$: C 56.70, H 3.57, N 4.96; found: C 56.61, H 3.50, N 4.87.

RESULTS AND DISCUSSION

Synthesis and Structural Characterization. The synthetic procedures for the N-donor ligands the and heteroleptic Pt^{II}(C^N)(N-donor ligand)Cl complexes are shown in Scheme 1 and 2. The cyclometalating ppy-type ligands **L-N**, **L-P** and **L-S** are synthesized by the reported method.[7] As the key compounds, the N-donor ligands are prepared from the Suzuki cross-coupling catalyzed by $Pd(PPh_3)_4$ between 4-bromopyridine hydrochloride and the corresponding borate compounds or boronic acid (**B-P**, **B-S** and **B-N**). The Pt^{II} complexes are obtained in high yields by a two-step protocol. The relevant cyclometalating ppy-type ligands reacted with K_2PtCl_4 to afford the μ-chloro-bridged dimer complexes, which are then converted to the final complexes by reaction with the N-donor ligands under mild condition. These air-stable compounds are isolated in high purity as solids by column chromatography on silica gel with the proper eluent.

Scheme 1. Synthesis Protocol for the Functional N-donor Ligands

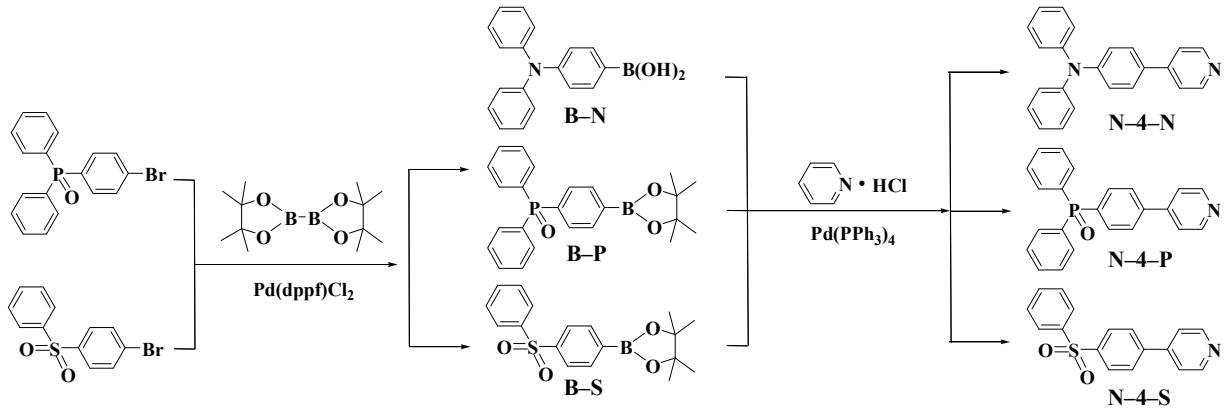

Scheme 2. Synthesis Protocol for the Pt^{II}(C^N)(N-donor ligand)Cl Complexes

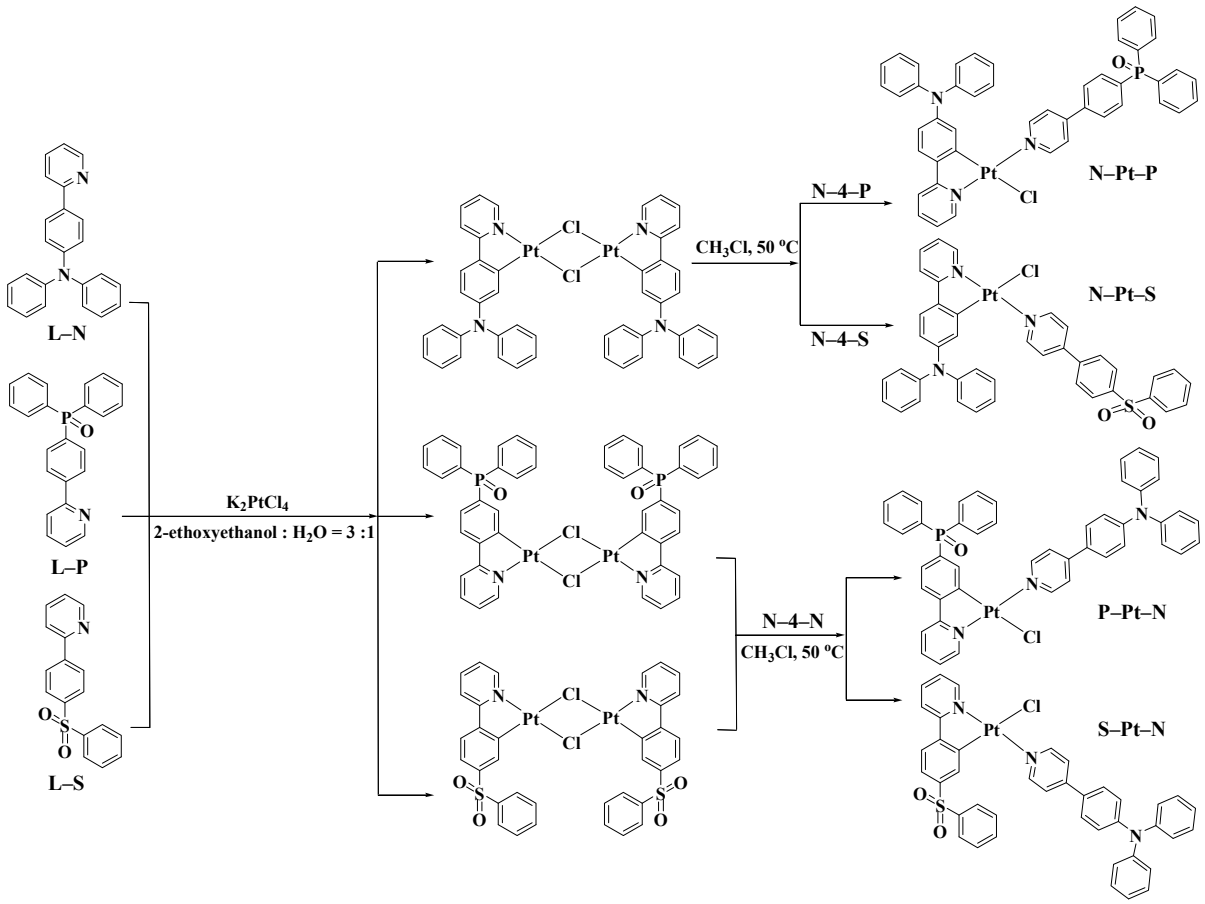

The ^{1}H, ^{13}C and ^{31}P NMR spectra of all compounds are thoroughly recorded. All the NMR spectra are provided in the SI (Fig S1, S2 and S3). In the ^{1}H NMR spectra for all the Pt^{II} complexes, the resonance signals with δ at *ca.* 9.58 (for **N-Pt-P** and **N-Pt-S**) and 9.75 ppm (for **P-Pt-N** and **S-Pt-N**)

can be assigned the protons adjacent to N atom on the pyridine ring of the cyclometalating ppy-type ligands. The resonance peaks with the chemical shift at *ca.* 8.65 to 8.79 ppm can be ascribed to protons in the proximity of the N atom on the pyridine ring of the N-donor ligands. The ratio of these two kinds of protons is 1 : 2, which is in good agreement with the structural features of these Pt^{II} complexes. The other resonance signals in the low field region come from the aromatic groups of cyclometalating ppy-type ligands and N-donor ligands. The resonance peak with δ at *ca.* 28.35 and 29.43 ppm in the ^{31}P NMR spectra of **N-Pt-P** and **P-Pt-N** can be assigned to the $–POPh_2$ groups, respectively. In addition, the MS spectra have been also collected to characterize the Pt^{II} complexes, which gave the respective molecular ion peaks clearly in Figure S4 (SI). At the meantime, single crystals of **S-Pt-N** were obtained by slow diffusion of its solution in $CHCl_3$/THF (v/v = 1 : 1) into hexane, and single X-ray crystallography was employed to investigated the structure of **S-Pt-N**. Its ORTEP drawing is illustrated in Figure 1, and the detailed structural data are summarized in Table S1 and S2 (SI). As shown in Figure 1, the Pt^{II} atom with a square planar coordination geometry is coordinated by a bidentate ppy-type ligand (**L-S**, C^N) and two monodentate ligands (N-donor ligand, **N-4-N** and chloride). The coordination around the Pt center is distorted tetragonal geometry with the *trans*-N, N and *trans*-C, Cl disposition. The bonds chelating around the Pt atom exhibit typical bond lengths comparing with some similar complexes.[48, 49] Generally, it can be concluded that the heteroleptic Pt^{II}(C^N)(N-donor ligand)Cl have been successfully prepared according to all of the spectral results and characterizations showing good consistency.

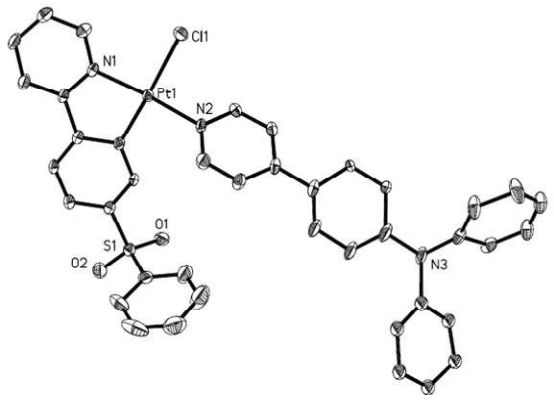

Figure 1. ORTEP drawing of **S-Pt-N** with thermal ellipsoids drawn at the 30% probability level. H atoms are omitted for clarity.

Thermal Properties and Photophysical Characterizations. The thermal properties of the heteroleptic Pt^{II}(C^N)(N-donor ligand)Cl complexes are investigated by thermogravimetric analysis (TGA) and different scanning calorimetry (DSC) under a nitrogen flow. The TGA results show their thermal stability with the decomposition temperature (T_d) in the range from *ca.* 303 to 326 ^oC (Table 1, Figure S5), which are similar to the Pt^{II}(C^N)acac type complexes.[7] The DSC traces have revealed their glass-transition temperature (T_g) in the range from *ca.* 109 to 128 ^oC (Table 1, Figure S6). The good thermal properties will guarantee their stability in fabrication and working process of the concerned EL devices.

Table 1 Photophysical and Thermal Data for the Heteroleptic Pt^{II}(C^N)(N-donor ligand)Cl Complexes.

Compd	Absorption [a] (293K) λabs (nm)	Emission λem (nm) solution [a] 293 K/77 K	Emission λem (nm) film PMMA [b]/neat	Φ 293 K solution [c] Φ_F/Φ_P	Φ 293 K film Φ_P [c] PMMA/neat	τ [d] solution 298 K/77 K	τ [d] film PMMA/neat	T_d/T_g (^oC)
N-Pt-P	255 (4.61), 274 (4.67), 338 (4.37), 377 (4.12), 426 (4.21)	447, 543/537	533/550	5.0%/4.7%	60.7%/45.1%	4.2 ns (447 nm) 0.3 μs (543 nm) /2.2 μs (537 nm)	1.1 μs (533 nm) /0.9 μs (550 nm)	325/122
N-Pt-S	253 (4.41), 274 (4.47), 341 (4.17), 380 (3.95), 423 (4.02)	450, 543/537	535/557, 580	6.5%/3.2%	68.0%/36.3%	3.8 ns (450 nm) 0.2 μs (543 nm) /2.3 μs (537 nm)	0.9 μs (535nm) /0.7 μs (557 nm)	315/128
P-Pt-N	252 (4.54), 293 (4.42), 328 (4.02), 390(4.53)	449, 502, 536 /503, 538	505, 541 /508, 547	5.6%/4.1%	57.1%/37.6%	4.6 ns (449 nm) 0.4 μs (502 nm) /1.9 (503 nm)	1.2 μs (505 nm) /0.8 μs (508 nm)	303/109
S-Pt-N	254 (4.57), 293 (4.48), 327 (4.09), 393 (4.58)	447, 503, 538 /507, 539	508, 544 /515, 550	7.8%/4.2%	72.0%/34.1%	4.7 ns (447 nm) 0.5 μs (503 nm) /2.1μs (507 nm)	1.3 μs (508 nm) /0.7 μs (515 nm)	326/117

[a] Measured in CH_2Cl_2 at a concentration of 10^{-5} M, log ε values are shown in parentheses. [b] Measured in PMMA film with 6 wt-% doping level. [c] Measured in degassed CH_2Cl_2 relative to *fac*-[Ir(ppy)$_3$] (Φ_P= 97%, λ_{ex}=360 nm),[50] the absolute Φ_Ps are obtained from Hamamstu Photonics K.K., E7536 model measurement system using their PMMA films with 6 wt-% doping level and neat films. [d] Measured in degassed CH_2Cl_2 solutions, films with a 369 nm picosecond LED as the excitation source.

UV-Vis absorption spectra for these Pt^{II} complexes are investigated in CH_2Cl_2 solution with a concentration of 10^{-5} mol L^{-1} at 293 K and the corresponding data are compiled in Table 1. As depicted in Figure 2, there are two main absorption bands in their UV-Vis spectra, showing similarity with respect to the reported results.[51] The first absorption bands can be safely assigned to the spin-allowed ligand-centered (LC) π-π* transition due to their large extinction coefficients (log ε >4).[18, 52] These Pt^{II} complexes present similar absorption behavior in the high-energy region before *ca.* 350 nm. The second absorption bands in low-energy region ranging from *ca*. 350 to 450 nm for these Pt^{II} complexes exhibit distinctive differences. The maximum absorption peaks for **P-Pt-N** and **S-Pt-N** are located at *ca*. 390 nm, which are obviously more intense than that of **N-Pt-P** and **N-Pt-S** centered at *ca.* 425 nm. To directly interpret the absorption behavior of these Pt^{II} complexes, the simulated UV-Vis spectra (Figure 3) with discrete vertical vibronic transitions and the time-dependent density functional theory (TD-DFT) calculations for all of these Pt^{II} complexes have been carried out. Figure 4 displays the distribution patterns of the highest occupied molecular orbitals (HOMOs), the lowest unoccupied molecular orbitals (LUMOs), HOMO-1 and LUMO+1. Table 2 summarizes the detailed TD-DFT results for these Pt^{II} complexes.

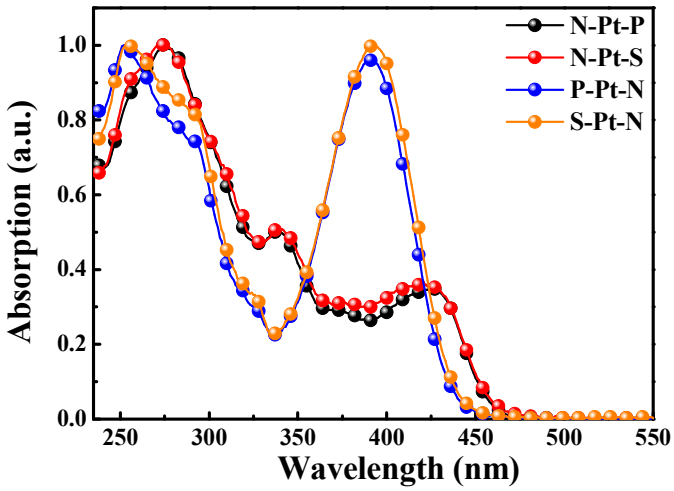

Figure 2. UV-Vis absorption spectra for these Pt^{II} complexes in CH_2Cl_2 at 293 K.

As displayed in Figure 3, the simulated UV-Vis spectra from theoretical calculations show excellent agreement with the experimental ones for all the Pt^{II} complexes in terms of both absorption wavelength and line-shape, indicating the validity of the calculation method. For **N-Pt-P** and **N-Pt-S**, the simulated UV-Vis results have shown that the low energy absorption bands located at *ca*. 425 nm with strong vertical vibronic transitions are from H→L+1 transition. As shown in Figure 4 and Table 2, the HOMOs for **N-Pt-P** and **N-Pt-S** are almost entirely located on the **L-N** ligand (96.77% and 97.07%, respectively, Table 2), while the LUMOs are mainly distributed on the N-donor ligands (94.36% for **N-4-P** and 96.32% for **N-4-S**, Table 2). The LUMO+1s are mainly contributed from the ppy moiety on the **L-N** ligands. Therefore, the absorption bands with low energy located at *ca*. 425 nm for **N-Pt-P** and **N-Pt-S** can be attributed to the intraligand charge transfer (ILCT) features from $–NPh_2$ moiety to ppy moiety within the **L-N** ligand. As for **P-Pt-N** and **S-Pt-N**, the obviously intense absorption bands centered at *ca*. 390 nm can be assigned to H→L and H→L+1 transitions with large percentage of vertical vibronic transitions. The N-donor ligand **N-4-N** gives a substantial contribution to the HOMOs for complexes **P-Pt-N** and **S-Pt-N** (98.39% and 98.69%, Table 2). The ppy units on the ligand **L-P** and **L-S** hold the primary distribution of their LUMOs and the 4-phenylpyridine unit on the ligand **N-4-N** gives the main contribution to the LUMO+1s. Consequently, ligand to ligand charge transfer (LLCT) transition (from **N-4-N** ligand to **L-P** and **L-S** ligands) and ILCT transition (from $–NPh_2$ moiety to 4-phenylpyridine moiety within the **N-4-N** ligand) should be responsible for the low energy absorption bands in the UV-Vis spectra of **P-Pt-N** and **S-Pt-N**. For all of these Pt^{II} complexes, the contribution from the d_π orbitals of Pt centers to their HOMOs is negligible (Table 2), which should result from the strong electron-donating property of $–NPh_2$ moiety, excluding the participation of the Pt^{II} center to the HOMO contribution.[45] So, no

noticeable MLCT transitions contribute to their UV-Vis spectra.

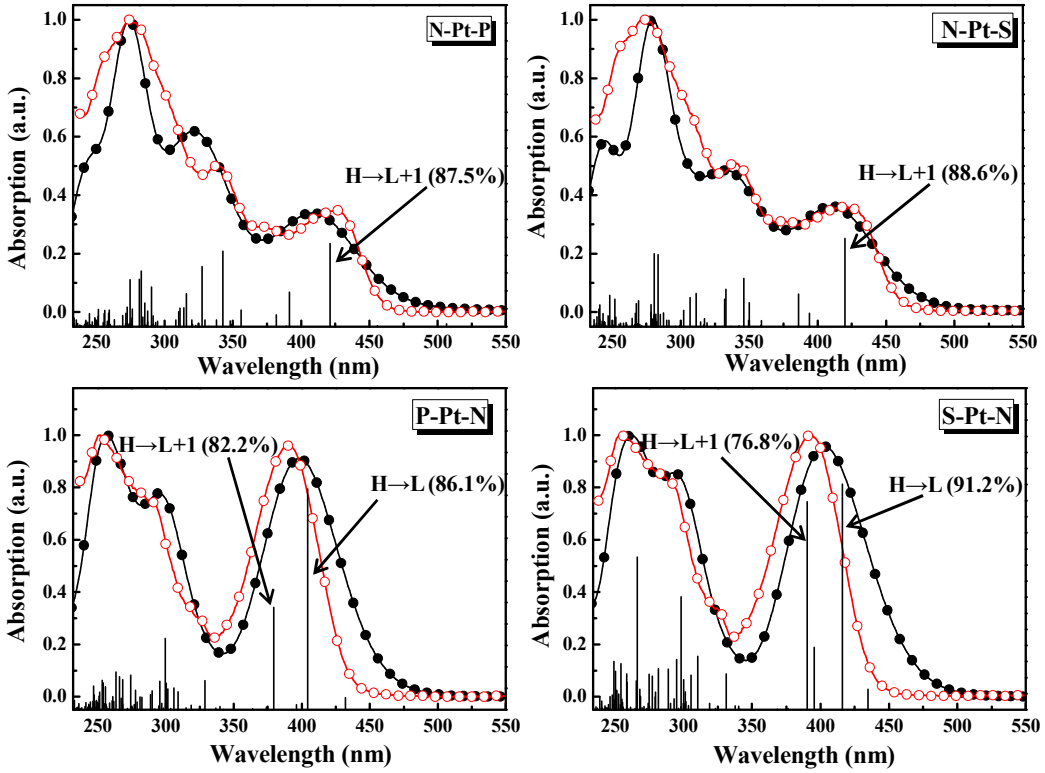

Figure 3. Experimental UV-Vis absorption spectra (red profile) and simulated spectra (black profile) with discrete vertical vibronic transitions for these Pt^{II} complexes.

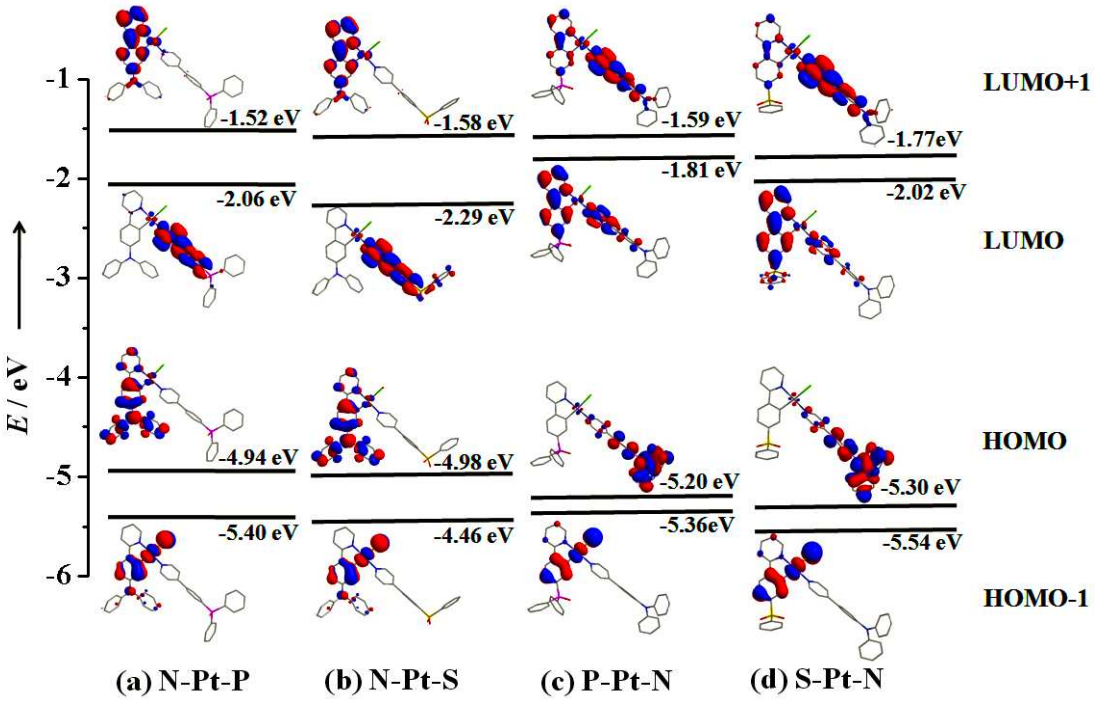

Figure 4. Molecular orbital (MO) patterns for these Pt^{II} complexes based on their optimized S_0

geometries

Table 2. TD-DFT Results for These Pt^{II} Complexes Based on Their Optimized S_0 Geometries

Complexes	MO	Contribution percentages of metal d_π orbitals and π orbitals of ligands to MOs (%)				Main configuration of $S_0 \rightarrow S_1$ excitation/E_{cal}/λ_{cal}/f [a]	Main configuration of $S_0 \rightarrow T_1$ excitation/E_{cal}/λ_{cal} [a]
		Pt	**L-N**	**N-4-P**	**Cl^-**		
N-Pt-P	L+1	5.25	90.35	4.06	0.33	H→L (98.4%)	H→L (37.1%), H→L+1 (50.7%)
	L	1.86	3.45	94.36	0.34	2.453 Ev	2.309 eV
	H	2.30	96.77	0.05	0.88	505 nm	537 nm
	H-1	34.98	31.23	0.14	33.65	0.0081	
		Pt	**L-N**	**N-4-S**	**Cl^-**		
N-Pt-S	L+1	5.17	90.40	4.08	0.34	H→L (98.8%)	H→L (74.8%), H→L+1 (20.0%)
	L	1.65	1.73	96.32	0.30	2.287 eV	2.237 eV
	H	2.11	97.07	0.05	0.77	542 nm	554 nm
	H-1	34.97	31.50	0.13	33.40	0.0045	
		Pt	**L-P**	**N-4-N**	**Cl^-**		
P-Pt-N	L+1	2.83	25.29	71.63	0.25	H→L (94.7%)	H→L (63.8%), H→L+1 (10.0%)
	L	3.73	69.77	26.03	0.47	2.869 eV	2.524 eV
	H	1.09	0.20	98.39	0.32	432 nm	491 nm
	H-1	36.36	28.28	0.36	35.00	0.0284	
		Pt	**L-S**	**N-4-N**	**Cl^-**		
S-Pt-N	L+1	2.34	15.79	81.63	0.24	H→L (95.4%)	H→L (59.3%), H→L+1 (12.2%)
	L	3.67	80.19	15.69	0.46	2.853 eV	2.490 eV
	H	0.92	0.16	98.69	0.23	435 nm	498 nm
	H-1	35.95	26.88	0.23	36.95	0.0315	

[a] H→L represents the HOMO to LUMO transition. E_{cal}, λ_{cal} and f represent calculated excitation energy, calculated absorption wavelength and oscillator strength, respectively. The oscillator strength of $S_0 \rightarrow T_1$ is zero due to the spin-forbidden of singlet-triplet transition under TD-DFT calculation in the Gaussian program without considering the spin-orbit coupling.

The PL spectra for these Pt^{II} complexes are recorded in both CH_2Cl_2 and film at 293 K. As displayed in Figure 5, all of these complexes emit much weaker luminescence in CH_2Cl_2 solutions compared with in films under irradiation with 365 nm UV light. In CH_2Cl_2 solutions (Figure 5a and S8), two types of emission bands can be observed. The emission bands located at *ca*. 450 nm for all Pt^{II} complexes should come from the ligand-centered (LC) π-π* transition. Due to the nanosecond scale lifetime (*ca*. 4 ns, Table 1), this high-energy emission band should be fluorescence induced by the singlet excited states (S_1).[36] On the contrary, the emission bands at longer wavelengths than 500

nm for these Pt^{II} complexes may be ascribed to the triplet excited state (T_1) emission for their much longer lifetime in the order of microseconds (Table 1).[51, 53] The phosphorescence intensities of these complexes are weaker than the fluorescence intensities, indicated by the lower phosphorescence quantum yield (Φ_p) than the fluorescence quantum yield (Φ_F) (Table 1). At room temperature (RT), in dilute solution, the d-d characters in excited states of the Pt^{II} chloride complexes are obvious due to the thermal activation.[54, 55] The low-lying metal-centered d-d excited states are rarely emissive because they provide a nonradiative pathway *via* molecule distortion in excited states attributed by the weak ligand field.[56, 57] Besides, the structural distortion from D_{4h} symmetry to D_{2d} symmetry of the square planar Pt^{II} complexes also results in nonradiative process, leading to low emission efficiencies in dilute solution.[5, 11, 56, 58] To support these point views, the PL properties of these complexes in dilute solution at 77 K are investigated. As shown in Figure 5b and S9, all of these Pt^{II} complexes exhibit highly strong phosphorescence emission, which is more than 10 times higher than at RT under the same measurement conditions, showing much longer phosphorescence lifetime of *ca*. 2.0 μs (Table 1). In cooperation with all the PL results in solutions, it can be drawn a conclusion that these Pt^{II} complexes emit intense fluorescence compared with the phosphorescence in CH_2Cl_2 solution at RT, which is due to the faster radiative decay rates of S_1 states than the T_1 states, induced by the free rotation of moieties, d-d metal-centered states and D_{4h} to D_{2d} structural distortions. However, at the low temperature of 77 K and in doped PMMA films, all these Pt^{II} complexes exhibit intense phosphorescence emission due to the rotational moieties and the structural distortions in excited states are efficiently restrained, promoting the radiative efficiency of the T_1 states (Table 1, Figure 5 and S9). Besides, the high efficiency of ISC process form S_1 to T_1 state is another reason for the strongly intense phosphorescence at 77 K.

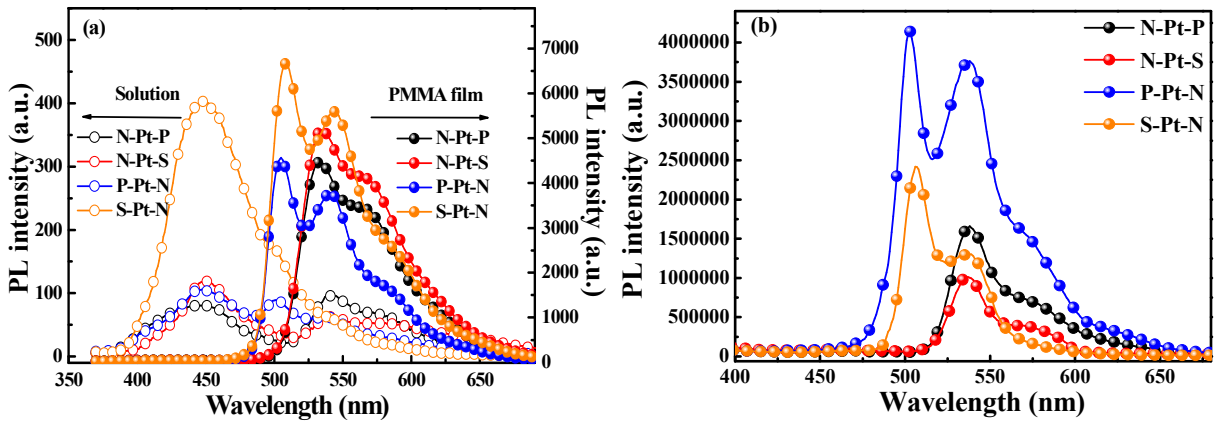

Figure 5. (a) PL spectra for all Pt^{II} complexes under same measurement conditions in CH_2Cl_2 solution at 293 K with a concentration of 10^{-5} M and in PMMA film with 6 wt-% doping level. (b) PL spectra for all Pt^{II} complexes in CH_2Cl_2 solution at 77 K with a concentration of 10^{-5} M.

With aim to clearly elucidate the PL behaviors of these Pt^{II} complexes, the natural transition orbitals (NTO) have been obtained based on the optimized T_1 geometries for their $S_0 \rightarrow T_1$ excitation. Figure 6 displays the NTO pattern and Table 3 presents the concerned NTO results for all of these Pt^{II} complexes. The NTO results for the **N-Pt-P** have shown that both hole (H) and particle (P) orbitals are mainly located on the ligand **L-N** (93.95% and 90.31%, respectively). Hence, the large percentage of H→P transition (98.70%) should suggest that ILCT transition process induces the phosphorescence emission of **N-Pt-P**. For **N-Pt-S**, the ligand **L-N** gives a major contribution to its hole and particle orbitals and the ligand **N-4-S** (17.75%) slightly contributes to its particle orbital as well. So, the ILCT-dominated transition together with slight LLCT features should account for the phosphorescent bands in the solution PL spectrum of **N-Pt-S**, showing agreement with its structured PL spectra (see Figure S8). From the data in Table 3, no noticeable MLCT transition process should be responsible for the phosphorescent signals in the PL spectra of **N-Pt-P** and **N-Pt-S** because of the negligible contribution of the Pt center in their NTOs (5.10% and 3.90%, respectively). Differently, in **P-Pt-N** and **S-Pt-N**, the Pt centers give some contribution to their hole orbitals (22.82% and 23.19%, respectively), while the ligand **L-P** and **L-S** predominantly accounts for the distributions of

both hole and particle orbitals (Figure 6 and Table 3). Consequently, the ILCT-dominated transition with some MLCT characters should be responsible for the phosphorescent feature of **P-Pt-N** and **S-Pt-N**. So, **P-Pt-N** and **S-Pt-N** can exhibit slightly less structured features in the line-shape of their phosphorescent spectra (Figure S8).

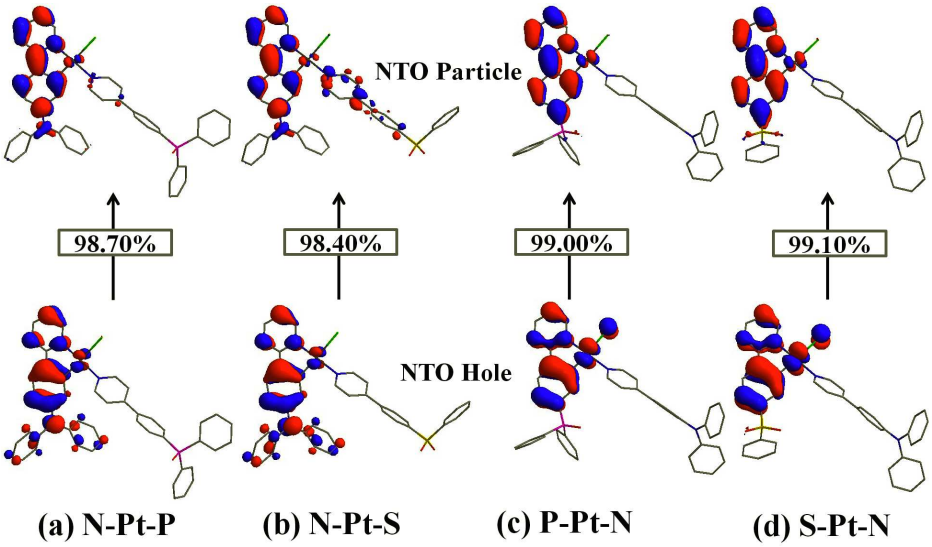

Figure 6. Natural transition orbital (NTO) patterns for $S_0 \rightarrow T_1$ excitation for these Pt^{II} complexes based on their optimized T_1 geometries.

Table 3. NTO Results for These Pt^{II} Complexes Based on Their Optimized T_1 Geometries.

Complexes	NTO[a]	Contribution percentages of metal d_π orbitals and π orbitals of ligands to NTOs (%)			
		Pt	**L-N**	**N-4-P**	**Cl**
N-Pt-P	H	5.10	93.95	0.11	0.84
	P	3.90	90.31	5.34	0.54
		Pt	**L-N**	**N-4-S**	**Cl**
N-Pt-S	H	4.92	94.05	0.12	0.92
	P	3.50	78.30	17.75	0.46
		Pt	**L-P**	**N-4-N**	**Cl**
P-Pt-N	H	22.82	69.82	0.11	7.25
	P	5.64	92.74	0.93	0.70
		Pt	**L-S**	**N-4-N**	**Cl**
S-Pt-N	H	23.19	68.74	0.10	7.97
	P	5.34	93.05	0.92	0.69

[a] H and P represent NTO hole and particle orbital, respectively.

The UV-Vis results and theoretical calculations reveal the obvious charge transfer (CT) character including the ILCT and LLCT features of the excited states in these Pt^{II} complexes, inducing solvatochromic effect in different polarity solvents. Therefore, the PL spectra of these Pt^{II} complexes in different solvents (toluene, CH_2Cl_2, THF, MeCN and DMF) have been investigated under the same measurement conditions. An obvious solvatochromic effect can be observed by changing the polarity of the solvents and these Pt^{II} complexes display structureless PL spectra in high polarity solvent (Figure 7), indicating the CT character of their excited states. Besides, the fluorescence bands are generally red-shifted with increasing the polarity of the solvents. In general, the phosphorescence intensity of these complexes is higher in the solvents with low polarity (toluene, CH_2Cl_2 and THF) than that in high polarity ones (MeCN and DMF) (Figure 7). Clearly, increasing the polarity of the solvent gives rarely positive effect on the phosphorescence enhancement of these complexes.

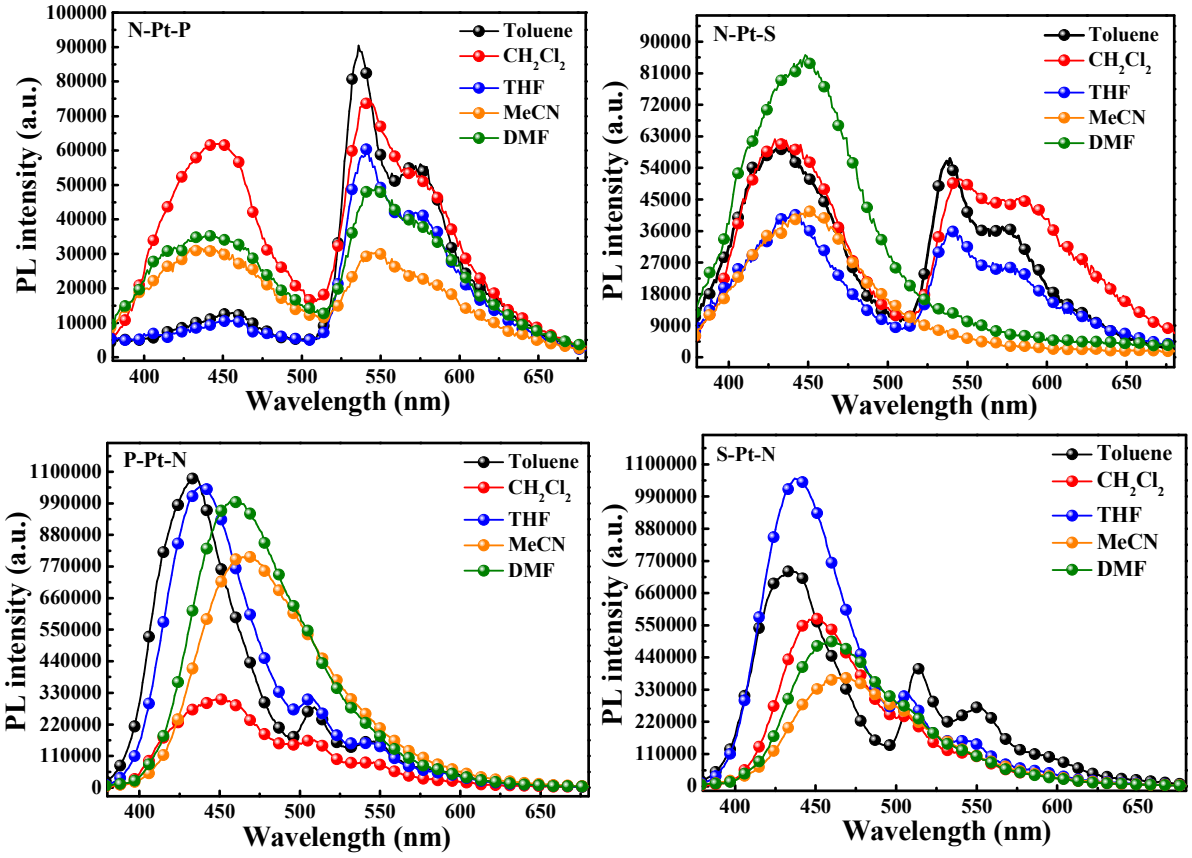

Figure 7. PL spectra for all Pt^{II} complexes under same measurement conditions in different solvents at 293 K with a concentration of 10^{-5} M

From the PL spectral difference in both rigid PMMA matrix and dilute solution (Figure 5a), it may suggest that the aggregation state makes a positive influence on enhancing the phosphorescent emission of these Pt^{II} complexes, *i.e.* these Pt^{II} complexes may be AIE-active. To confirm the AIE property of these Pt^{II} complexes, the PL spectra of these Pt^{II} complexes in tetrahydrofuran-water (THF-H_2O) mixture with different H_2O volumetric fractions (f_w) have been measured (Figure 8). For **N-Pt-P**, two main emission peaks located at *ca*. 470 nm and 530 nm can be observed in THF solution. With increasing the f_w, the PL intensities for the two peaks are increasing as well. When the f_w reaches 80%, the fluorescence emission signal at 470 nm starts to decrease, while the phosphorescent emission band centered at 530 nm is greatly increased. At the f_w of 90%, the emission signal for the peak of 470 nm has nearly disappeared, only the emission at 530 nm can be observed, showing a peak PL intensity of *ca*. 10 times higher than that of in THF solution. As for **N-Pt-S**, similar emission peaks located at *ca*. 470 nm and 530 nm can be detected in THF solution as well. With increasing the f_w, the PL intensities for the two peaks initially increase (f_w = 10% and 20%), and then begin to decrease with the f_w of 30%. When the f_w increases to 90%, the fluorescent emission signal for the peak at 470 nm is absent, only the phosphorescence emission peak at 530 nm can be detected with much higher intensity than that in THF solution. As for **P-Pt-N** and **S-Pt-N**, only one main emission peak at *ca*. 445 nm can be obviously observed in their THF solution. When the f_w is 10%, the PL intensities are the highest. Starting from the f_w of 20%, the emission peaks at *ca*. 445 nm are red-shifted to *ca*. 470 nm with PL intensity decreasing. At the f_w of 90%, the phosphorescence signal can be detected for **P-Pt-N** and **S-Pt-N** with the similar intensity comparable to that of **N-Pt-S** (Figure 8).

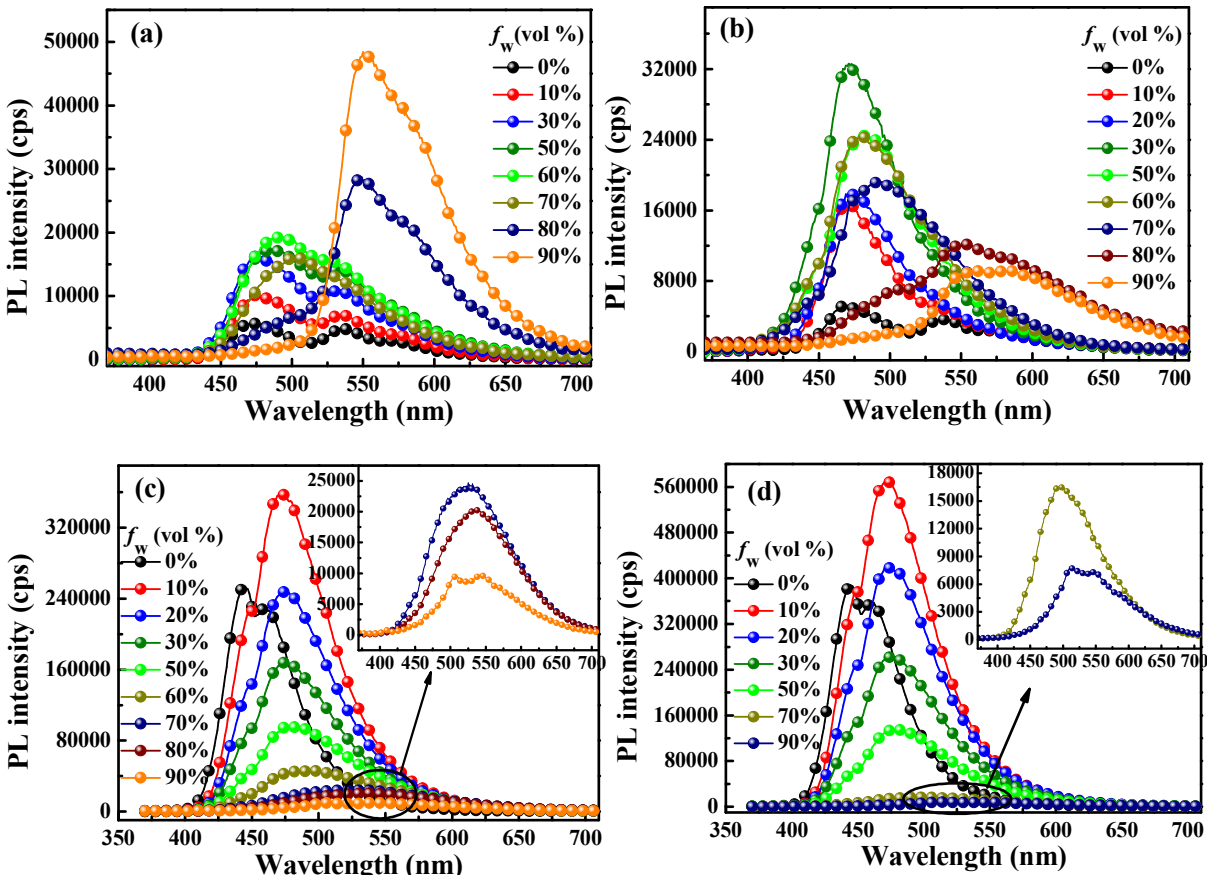

Figure 8. PL spectra in THF-H_2O mixture with different H_2O volumetric fractions under same measurement condition ((a) for **N-Pt-P**, (b) for **N-Pt-S**, (c) for **P-Pt-N** and (d) for **S-Pt-N**, when f_w = 0%, concentration is 2× 10^{-4} M).

Suggested by the data in Figure 7, increasing the polarity of solvent cannot show positive effect on enhancing the phosphorescence intensities of these complexes. As the f_w increasing, the polarity of the mixed solvent (THF-H_2O) rises up as well. However, in Figure 8, the emission intensities are obviously enhanced. Hence, the solvatochromic effect on the emission enhancements of these complexes in different THF-H_2O mixture should be excluded. The emission intensity enhancements in the THF-H_2O mixture of these complexes should be attributed to the aggregates generated by adding water. To verify this perspective, the absorption behavior of these complexes in the mixture of THF and H_2O has been characterized. As shown in Figure 9, from 10% to 70% of f_w, no obvious

changes in absorption wavelength are observed. As the f_w increasing to 90%, the absorption bands are red-shifted to longer wavelength region. Besides, the low-energy absorption bands show a level-off tail feature due to the light-scattering effects of aggregates formed in the mixed solvent. Clearly, after these Pt^{II} complexes aggregated in the mixture with increasing H_2O contents, the concentration of the dissolved Pt^{II} complex is greatly decreased, resulting in the inefficiency of light absorption.[59] As a result, these complexes show a decreasing absorption intensities when the f_w increases. Many research results based on both AIE-active organic compounds and Pt^{II} complexes have proved that the nano-aggregate suspensions of these compounds generated in high f_w conditions should induce both the red-shift effect and level-off tail in their UV-Vis spectra due to the light-scattering effect of the formed aggregates.[23, 31, 33, 35, 60, 61] To confirm the existence of nano-aggregates with the f_w increasing, the dynamic light scattering (DLS) experiments for these complexes have been studied using the mixture at the f_w of 90%. DLS results reveal that the aggregates with average diameter of less than 200 nm are formed in the medium of 90% f_w (Figure S11). Based on both the PL and UV-Vis results in same THF : H_2O mixture, together with the DLS results at the f_w of 90% mixture, it can be concluded that the nano-aggregates of these Pt^{II} complexes have been generated in THF : H_2O system with the f_w increasing, they are the main reason behind the PL enhancement in Figure 8.

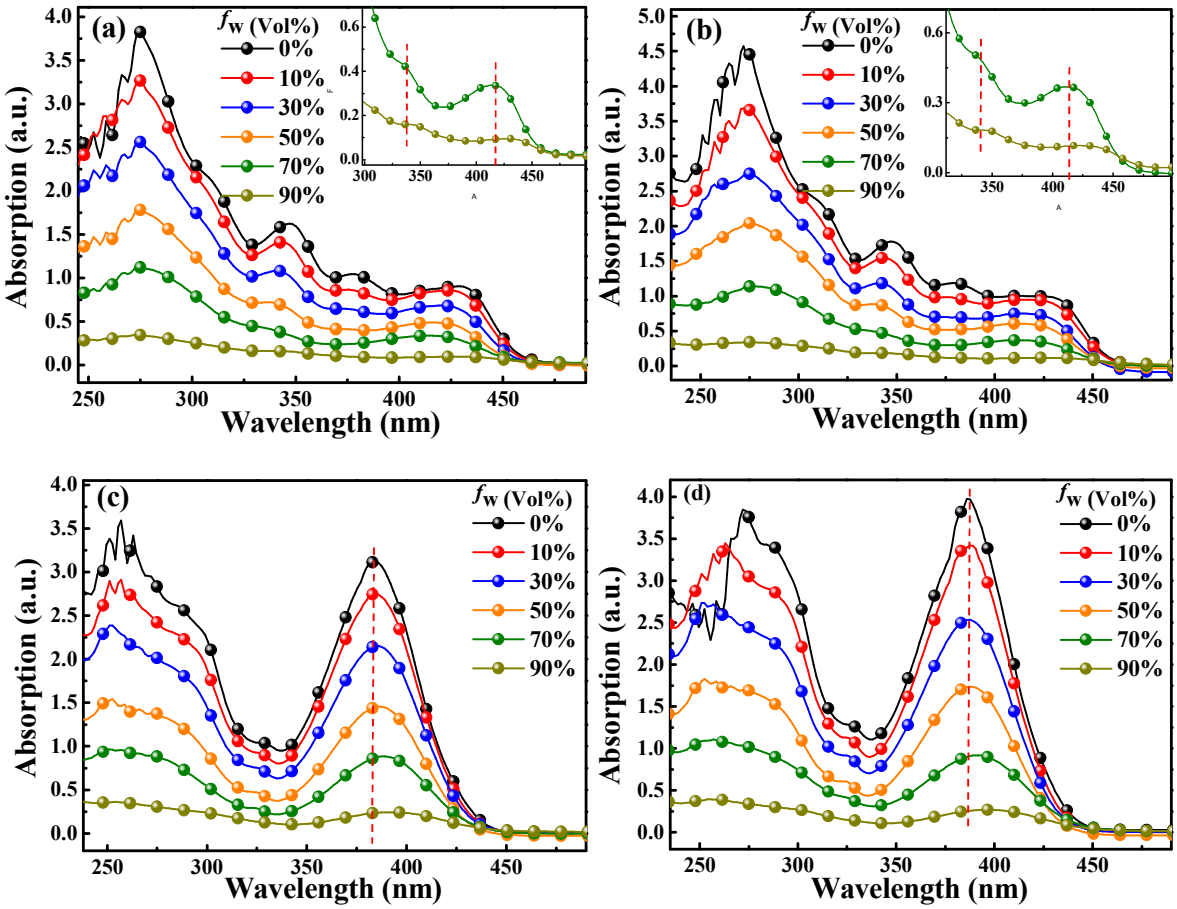

Figure 9. UV-Vis spectra in THF-H_2O mixture with different H_2O volumetric fractions under same measurement conditions ((a) for **N-Pt-P**, (b) for **N-Pt-S**, (c) for **P-Pt-N** and (d) for **S-Pt-N**, when f_w = 0%, concentration is 7.9× 10^{-5} M).

By restraining the rotational N-donor ligands **N-4-P** and **N-4-S** as well as the –NPh_2 moiety on ligand **L-N** in the aggregated state, the enhanced radiative decay of the T_1 states can account for the obvious phosphorescence enhancement with the increasing of f_w in the solutions of **N-Pt-P** and **N-Pt-S** (Figure 8). On the contrary, the **P-Pt-N** and **S-Pt-N** exhibit lower phosphorescence enhancement, the lower molecular aggregation degree in the THF-H_2O system should be responsible for this result. The intramolecular rotation and D_{4h} to D_{2d} distortion become much easier due to the lower molecular aggregation degree of **P-Pt-N** and **S-Pt-N** in THF-H_2O system, resulting in lower phosphorescence emission induced by T_1 states. Even though, the phosphorescence intensity of

P-Pt-N and **S-Pt-N** is still in the similar order to that of **N-Pt-S** (Figure 8). In short, the PL results in different THF-H_2O mixture should prove that these Pt^{II} complexes are AIE-active.

Clearly indicated by Figure 8, all complexes initially exhibit a fluorescent intensity enhancement in the THF-H_2O system with lower f_w and then the phosphorescence emission increases with the f_w increasing. It indicates that the phosphorescent emission enhancement should need much higher aggregation degree among the molecules of these Pt^{II} complexes to more effectively restrain the rotation of both N-donor ligand and functional groups, guaranteeing much higher radiative efficiency of the T_1 states.

As is well known, the phosphorescent materials employed in OLEDs are typically doped into a solid matrix, *i.e.* host material. Hence, it is more desirable that the AIE behaviors of these Pt^{II} complexes should be investigated in doped film to evaluate its potential in EL field. On this basis, these Pt^{II} complexes have been doped with PMMA with doping level of 6 wt-%, 10 wt-%, 20 wt-%, 40 wt-% and 60 wt-%, these doped PMMA films and their neat films are employed to characterize their AIE properties. The non-emissive PMMA has been selected as rigid matrix to avoid the effect of host-to-guest energy-transfer on the phosphorescent intensity which is also generated by the AIE process as aforementioned. As depicted in Figure 5a, 10 and S10, all of these Pt^{II} complexes emit intense phosphorescence emission in films. From the doping level of 6% to 10% or/and 20%, these Pt^{II} complexes show obvious enhancement in the phosphorescence intensity. Continuously increasing the doping level to 40%, the phosphorescence intensities of these complexes begin to decrease and reach the lowest in the neat films. In addition, the phosphorescence lifetimes also low down with increasing the contents of the Pt^{II} complexes. These PL results should indicate the structural distortion (D_{4h} to D_{2d}) in excited state of these Pt^{II} complexes.

Cleary indicated by the PL results in films, the restrictions of the rotational moieties and the D_{4h} to D_{2d} distortions can be relayed on the PMMA content. In the doped films with high PMMA contents *i.e.* low doping level of the Pt^{II} complex, the structural distortion in excited states of these complexes can be greatly restrained by the PMMA matrix. So, the radiative decay of the T_1 states is more efficient, achieving obviously stronger phosphorescence. Besides, the restraint of the rotational moieties in these complexes also promotes the radiative decay of the T_1 states. However, with low PMMA contents *i.e.* high doping level of the Pt^{II} complex, the rotations of the moieties in these complexes and the structural distortions become much easier, the T_1 states prefer to the nonradiative decay process, leading to the lower phosphorescence intensity. Of course, the triplet-triplet quenching might also be one of the possible reasons to induce lower phosphorescence intensity of the films with high dopant contents.[5, 11] The much shorter phosphorescence lifetimes of these complexes in films with the doping level of 40%, 60% and neat films than that of in 6%, 10 % and 20 % films should represent a good support. The neat films can still receive the highest Φ_p of *ca*. 45.0%, still showing nearly 10 times higher than these in dilute solutions. In the doped films at doping level of 6 wt.%, the phosphorescence intensity is increased by *ca*. 45- to 50-fold compared with that of in CH_2Cl_2 solutions (Figure 5a). The **S-Pt-N** exhibits the highest Φ_p of *ca*. 72.0% among all these Pt^{II} complexes. The Φ_p for **N-Pt-S** is 68.0%, which is 21.5 times higher than that of its dilute solution. All these inspiring PL results suggest that these Pt^{II} complexes are AIE-active. This AIE nature also can be confirmed by the vivid image comparison of the luminescence between in solution and PMMA film (Figure 5a). The phosphorescence of these complexes is obviously enhanced in the solid state. Furthermore, they possess much higher AIE ability in the doped film, which should be favorable for OLED application.

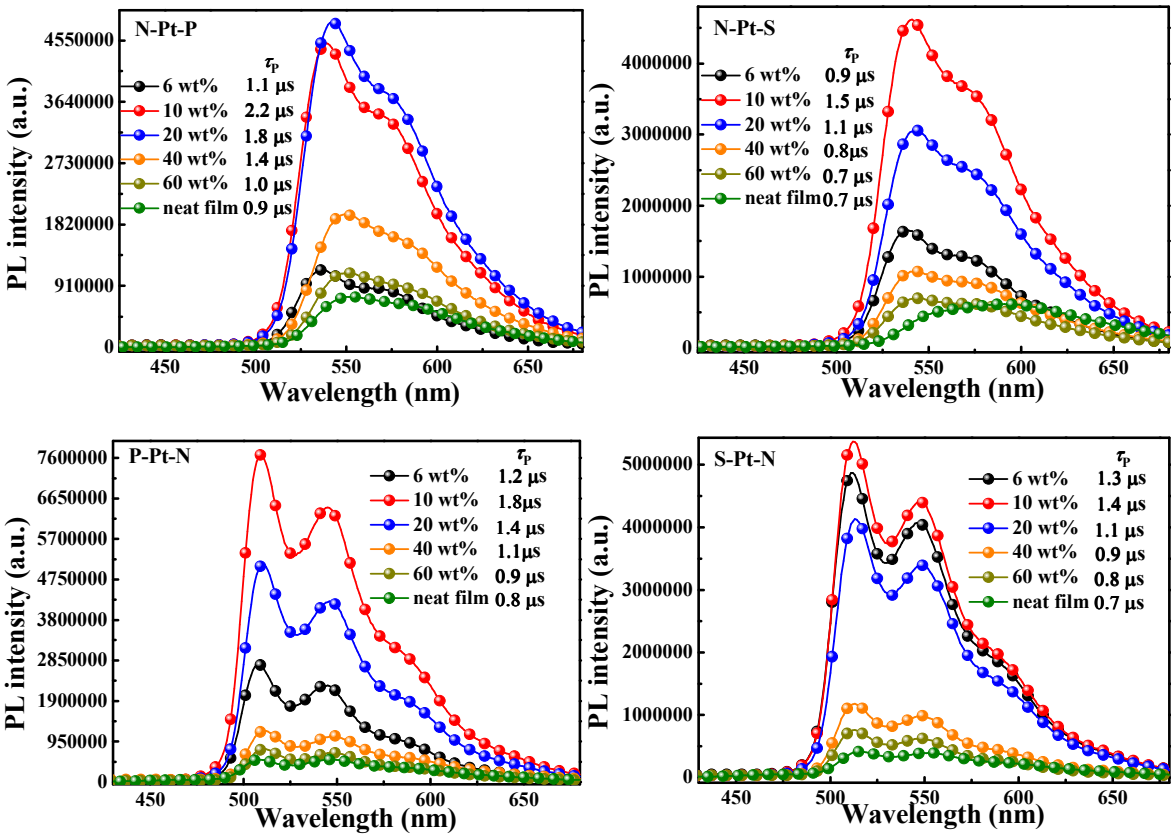

Figure 10. PL spectra for these Pt^{II} complexes in different doping rate PMMA films and neat films.

As is well-established, the restrained intramolecular rotation (RIR) can be a reasonable mechanism for the AIE nature (Figure 11).[23] In aggregated or solid state, the rotation of the N-donor ligands along with the $–NPh_2$, $–POPh_2$ and $–SO_2Ph$ moieties in the cyclometalating ligand can be effectively restrained by the rigid PMMA matrix or the Pt^{II} complexes themselves. Hence, these complexes in aggregated or solid state, the RIR effect inhibits the nonradiative decay process, and enhances the radiative decay of the T_1 states, achieving strong phosphorescence emission. As is well known, such as increasing solvent viscosity and decreasing solution temperature, these external controls exhibit positive effect on the restraint of the intramolecular rotation.[62] For these Pt^{II} complexes, the obvious phosphorescence enhancements at 77 K should provide a good support for this RIR effect due to the rotating units are restrained at low temperature (Figure 5b and S9). Besides, the rotating units in

these complexes also can be efficiently restrained by increasing of solvent viscosity according to the obvious phosphorescence enhancements obtained from the PL investigation of the dilute solutions (10^{-5} M) under different viscosity conditions (Figure S12). Taking all the PL results into consideration, the RIR effect together with restrained structural distortion should be the main reason for these Pt^{II} complexes showing very strong phosphorescent emission in the aggregated or solid state.

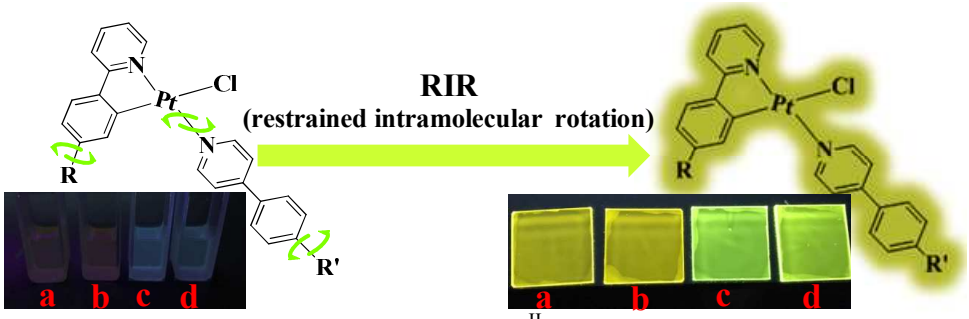

Figure 11. Mechanism for the concerned AIE-active Pt^{II} complexes and the PL luminescence images under 365 nm light illumination in a concentration of 10^{-5} M together with PMMA film with a doping of 6 wt-%: (a) for **N-Pt-P**, (b) for **N-Pt-S**, (c) for **P-Pt-N** and (d) for **S-Pt-N**.

Electrochemical Properties

Under nitrogen atmosphere in an acetonitrile solution, the cyclic voltammetry (CV) calibrated against the ferrocene/ferrocenium (Fc/Fc^+) redox couple as an internal reference has been applied to characterize the electrochemical properties of these Pt^{II} complexes. The results are presented in Table 4 and Figure S7. In the anodic scan, the first oxidation potential (E_{pa}) with reversible feature ranging from *ca*. 0.36 to 0.48 V can be assigned to the oxidation of the electron-rich $–NPh_2$ moiety,[7, 63, 64] which is absent in their parent complex **ppy-Pt-py**. The **N-Pt-P** shows the lowest E_{pa} at *ca*. 0.36 V due to the d_π-π conjugation effect with the Pt center (Table 2). Besides, the second irreversible oxidation potential ranging from *ca*. 0.57 to 0.67 V can be ascribed to the oxidation of the Pt center in these complexes, since it is similar to the reported results for other Pt^{II} complexes.[7, 18, 65, 66] In

associating with the E_{pa} results, the good hole injection (HI) ability should be conferred to these Pt^{II} complexes owing to their much lower E_{pa} than that of the parent complex **ppy-Pt-py**.

In the cathodic scan, all of these Pt^{II} complexes exhibit two reduction waves. The first cathodic peak potential (E_{pc}) at *ca*. -2.03 V should come from the reduction of the $–POPh_2$ or $–SO_2Ph$ moieties in these complexes (-2.03 V and -2.24 V for $–POPh_2$ group in **N-Pt-P** and **P-Pt-N**, -2.21 V and -2.37 V for $–SO_2Ph$ moiety in **N-Pt-S** and **S-Pt-N**, respectively).[47, 67] In addition, the reduction peaks in the more negative region at *ca.* -2.50 V can be assigned to the reduction of pyridyl group in the complexes. These data are similar to that of **ppy-Pt-py** and the reported results.[47] As a result, the LUMO levels of these complexes range from *ca*. -2.43 to -2.77 eV and are much lower than those of their parent complex **ppy-Pt-py** and the reported Pt(ppy)acac type complexes,[7] The concerned results indicate that the $–POPh_2$ or $–SO_2Ph$ functional moieties should offer good electron-injection (EI) abilities to these Pt^{II} complexes. Taking both of the oxidation and reduction results into consideration, the functional groups $–NPh_2$, $–POPh_2$ and $–SO_2Ph$ should endow these Pt^{II} complexes with good charge carrier injection ability, which can be very desirable for improving the EL performance of the concerned Pt^{II} complexes.

Table 4. Electrochemical Properties for the Pt^{II} Complexes.

Compounds	E_{pa} (V)	E_{pc} (V) [b]	HOMO (eV) [c]	LUMO (eV) [d]	E_g (eV) [e]
N-Pt-P	0.36 [a], 0.61 [b]	-2.03, -2.44	-5.16	-2.77	2.39
N-Pt-S	0.44 [a], 0.57 [b]	-2.21, -2.49	-5.24	-2.59	2.65
P-Pt-N	0.40 [a], 0.62 [b]	-2.24, -2.52	-5.20	-2.56	2.64
S-Pt-N	0.48 [a], 0.67 [b]	-2.37, -2.64	-5.28	-2.43	2.85
ppy-Pt-py	0.83 [b]	-2.40	-5.63	-2.40	3.23

[a] Reversible. The value was set as $E_{1/2}$. [b] Irreversible or quasi-reversible. The value was derived from the cathodic peak potential. [c] HOMO levels are calculated according to the first oxidation potential from CV data, HOMO = - (E_{pa} + 4.8) eV. [d] LUMO levels are obtained from the onset potential of the first reduction wave from the CV data, LUMO = - (E_{pc} + 4.8) eV. [e] CV energy gap E_g = LUMO – HOMO.

Electroluminescent Properties

To verify the EL properties of these Pt^{II} complexes, solution-processed OLEDs have been fabricated with the configuration of ITO/PEDOT:PSS (45 nm)/emission layer, EML Pt x%:CBP (40 nm)/TPBi (45 nm)/LiF (1 nm)/Al (100 nm) (Figure 12). The PEDOT:PSS layer is employed as hole injection layer (HIL). The 4,4'-*N*,*N*'-'dicarbazole-biphenyl (CBP) layer is host material. The 1,3,5-*tris*-(*N*-(phenyl)-benzimidazole)-benzene (TPBi) layer serves as both hole-blocking and electron-transporting, while LiF acts as an electron-injection layer. In order to avoid the ACQ effect and optimize the EL performance of the OLEDs, variation of the doping levels has been carried out in device fabrication.

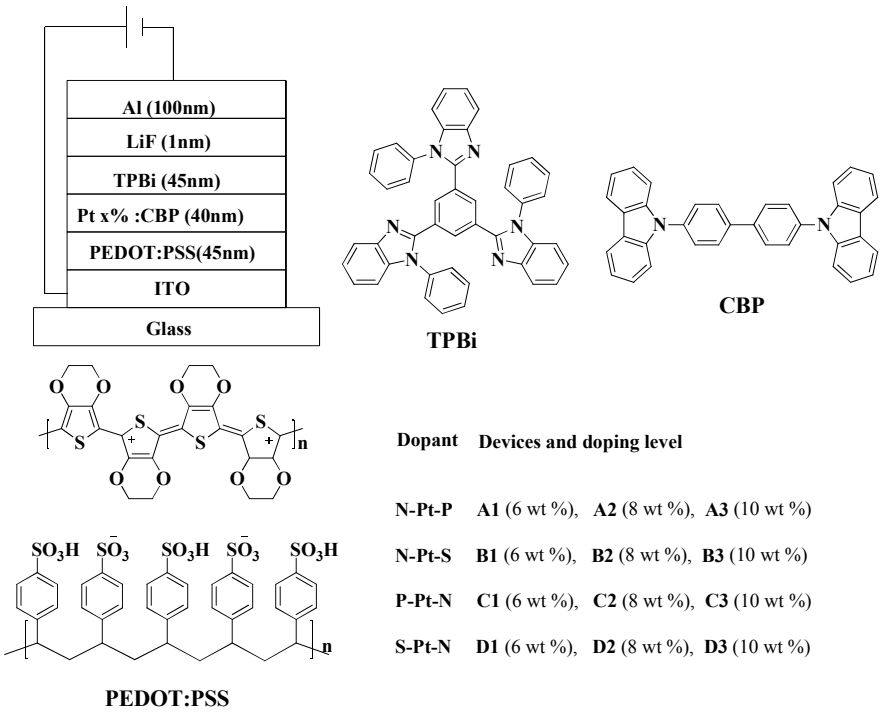

Figure 12. Configuration of the OLEDs made from these Pt^{II} complexes and the chemical structures for the functional materials involved.

Table 5. EL Performance of the Solution-Processed OLEDs.

Device	Dopant	$V_{turn\text{-}on}$ (V)	Luminance L_{max} (cd m^{-2}) [a]	η_{ext} (%)	η_L (cd A^{-1})	η_p (lm W^{-1})	λ_{max} (nm) [d]
A1	**N-Pt-P** (6.0 wt-%)	3.6	17569 (16.7)	20.5 (5.3) [a] 19.9 [b] 15.6 [c]	57.5 (5.3) 55.7 43.8	42.7 (3.9) 28.6 17.0	535 (0.40, 0.59)
A2	**N-Pt-P** (8.0 wt-%)	3.9	18575 (16.9)	23.2 (5.2) 22.9 17.9	64.9 (5.5) 64.4 50.2	46.5 (3.9) 34.7 20.2	535 (0.40, 0.59)
A3	**N-Pt-P** (10.0 wt-%)	3.9	16937 (17.3)	22.0 (5.0) 20.6 15.0	61.8 (5.0) 57.8 42.2	44.8 (3.9) 29.7 16.4	535 (0.40, 0.59)
B1	**N-Pt-S** (6.0 wt-%)	3.5	12686 (18.1)	16.9 (5.1) 16.3 12.3	47.2 (5.1) 45.5 34.3	38.1(3.5) 22.8 12.3	535 (0.39, 0.59)
B2	**N-Pt-S** (8.0 wt-%)	3.4	13874 (19.7)	19.4 (4.8) 18.2 13.6	54.0 (4.8) 50.9 38.1	43.0 (3.4) 23.6 12.5	535 (0.39, 0.59)
B3	**N-Pt-S** (10.0 wt-%)	3.4	13017 (19.4)	17.8 (5.4) 17.3 12.3	49.8 (5.4) 48.4 34.4	37.4 (3.4) 24.5 12.0	535 (0.39, 0.59)
C1	**P-Pt-N** (6.0 wt-%)	4.9	13332 (13.8)	15.4 (5.9) 14.8 12.6	40.7 (5.9) 39.3 33.4	23.7 (5.1) 18.1 13.2	506, 540 (0.32, 0.61)
C2	**P-Pt-N** (8.0 wt-%)	3.7	15163 (13.8)	21.7 (4.9) 20.2 16.1	57.4 (4.9) 53.4 42.6	44.7(3.7) 28.0 18.1	506, 540 (0.32, 0.61)
C3	**P-Pt-N** (10.0 wt-%)	4.3	12978 (13.0)	11.3 (5.2) 10.9 9.2	29.8 (5.2) 28.9 24.2	19.7 (4.6) 15.8 11.1	506, 540 (0.32, 0.61)
D1	**S-Pt-N** (6.0 wt-%)	3.7	13912 (14.4)	27.8 (4.9) 26.5 19.8	74.1 (4.9) 70.8 53.0	58.3 (3.7) 41.0 23.4	512, 544 (0.33, 0.61)
D2	**S-Pt-N** (6.0 wt-%)	3.6	13926 (14.5)	28.4 (4.2) 26.4 19.3	75.9 (4.2) 70.4 51.5	62.7 (3.6) 41.9 23.2	512, 544 (0.33, 0.61)
D3	**S-Pt-N** (10.0 wt-%)	3.7	13787 (15.3)	20.1 (4.9) 18.8 14.1	53.9(4.9) 50.2 37.7	42.1 (3.7) 27.7 15.4	512, 544 (0.33, 0.61)

[a] Maximal values of the devices. Values in parentheses are the voltages at which date were obtained. [b] Values were collected at 100 cd m^{-2}.[c] Values collected at 1000 cd m^{-2}. [d] Values were collected at 8 V and CIE coordinates (x, y) are shown in parentheses.

After applying a proper voltage, these OLEDs exhibited intense green to yellow electroluminescence. The turn-on voltages of these devices are relatively low, ranging from *ca*. 3.4 to 4.9 V (Table 5). As displayed in Figure 13, the EL spectral profile of each optimized device is virtually identical to the spectrum of the corresponding Pt^{II} complex in the PMMA film (Figure 5a and 10), suggesting that EL emission indeed originates from the triplet excited states of the Pt^{II}

complexes. Additionally, no residual emission from CBP is observed in these devices even at the 6 wt-% doping level, implying the efficient forward energy transfer from the host excitons to the phosphorescent dopants and effective confinement of the excitons on the Pt^{II} complexes to guarantee the high EL efficiencies.

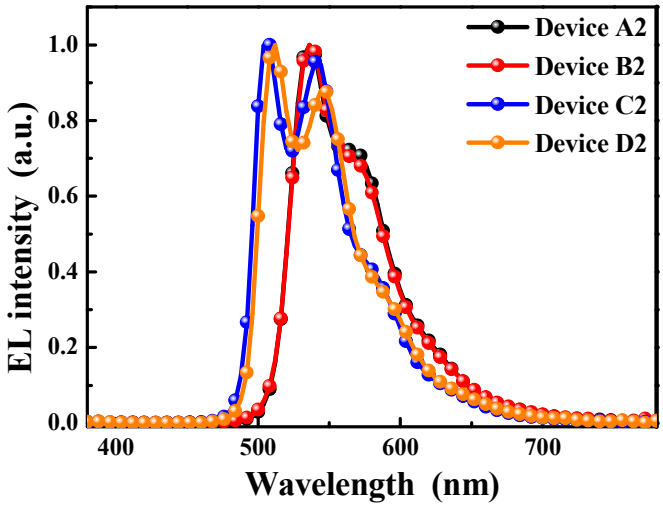

Figure 13. EL spectra for the optimized devices at *ca*. 10 V.

The current density–voltage–luminance (*J*–*V*–*L*) relationships and EL efficiency–luminance curves are displayed in Figure 14 and 15 along with Figure S13 and S14 (SI). Table 5 presents their EL data of these Pt^{II} complexes. From the data in Table 5, among all the devices, device **D2** based on **S-Pt-N** at a doping level of 8 wt-% shows the best EL efficiency with a peak luminance (L_{max}) of 13926 cd m^{-2} at *ca*. 14.5 V, a maximal external quantum efficiency (η_{ext}) of 28.4%, a maximal current efficiency (η_L) of 75.9 cd A^{-1} and a maximal power efficiency (η_P) of 62.7 lm W^{-1} (Table 5). Device **A2** constructed by **N-Pt-P** also showed competitive EL performance with L_{max} of 18575 cd m^{-2}, η_{ext} of 23.2%, η_L of 64.9 cd A^{-1} and η_P of 46.5 lm W^{-1}. These impressive EL results should be closely connected with the design concept that introduction of the $–NPh_2$, $–SO_2Ph$ and $–POPh_2$ functional moieties can provide enhanced charge carrier injection/transporting ability to the concerned Pt^{II}

complexes for improving their EL efficiency. To evaluate this idea, the single charge carrier devices have been fabricated from **S-Pt-N** and **N-Pt-P** in neat film considering their better EL efficiencies (Figure 16). For the hole-only devices, the hole current density of **S-Pt-N** and **N-Pt-P** with $–NPh_2$ moiety is higher than their parent complex **ppy-Pt-py** (Figure 16). So, the introduction of $–NPh_2$ moiety can definitely facilitate the hole-transporting ability of the concerned Pt^{II} complexes. For the electron-only devices, the parent complex **ppy-Pt-py**, **S-Pt-N** and **N-Pt-P** show high electron current density. However, the electron current density for **S-Pt-N** and **N-Pt-P** is lower than that of **ppy-Pt-py**. It may indicate that **S-Pt-N** and **N-Pt-P** show good electron-trapping ability. Consequently, the holes form the anode can easily recombined with the trapped electrons on **N-Pt-P** and **S-Pt-N** to realize high recombination efficiency and hence achieve high EL performance. According to the aforementioned CV results, these Pt^{II} complexes bearing $–NPh_2$, $–SO_2Ph$ and $–POPh_2$ can show good hole and electron injection abilities. As a result, these Pt^{II} complexes can exhibit advanced electron and hole injection/transporting ability (*i.e.* ambipolar feature). It certainly demonstrates that the good charge carrier injection/transporting ability is the important reason for the impressive EL performance of these Pt^{II} complexes.

It's well accepted that the Φ_p plays a key role in achieving high EL performance of the emissive materials. The PL investigation has proven that these Pt^{II} complexes are AIE-active, exhibiting relatively high Φ_p in PMMA films (Table 1). Hence, the AIE-nature should be another reason behind the good EL performance of these Pt^{II} complexes. Among these Pt^{II} complexes, **S-Pt-N** exhibits the best AIE nature with highest Φ_p in PMMA film (*ca*. 72.0%), which should be the reason for its excellent EL performance with respect to the other Pt^{II} complexes (Table 5). By taking **S-Pt-N** and **N-Pt-P** into comparison, the Φ_p for **N-Pt-P** (60.7%) is lower than that of **S-Pt-N** in PMMA film

(Table 1). In addition, the molecular interaction among **N-Pt-P** induced by the strong polarity –$POPh_2$ moiety may cause some exciton quenching problem. As a result, the EL performance of device **A2** fabricated by **N-Pt-P** is inferior to device **D2** based on **S-Pt-N** (Table 5).

For **N-Pt-S** and **S-Pt-N**, the molecular dimension for N-donor ligand **N-4-S** bearing –SO_2Ph group is much smaller than its counterpart ligand **N-4-N** with –NPh_2 unit. So, the ligand **N-4-S** with smaller –SO_2Ph group should be more rotational. Accordingly, the **N-Pt-S** should exhibit lower rigidity with respect to **S-Pt-N**. Consequently, **N-Pt-S** bearing the more rotational ligand **N-4-S** should exhibit lower AIE activity indicated by its lower Φ_p of 68.0% with respective to **S-Pt-N** (72.0%, Table 1). As a result, to compare with device **D2** based on **S-Pt-N**, the device **B2** with **N-Pt-S** as emitter exhibits lower EL efficiencies with L_{max} of 13874 cd m^{-2}, η_{ext} of 19.4%, η_L of 54.0 cd A^{-1} and η_P of 43.0 lm W^{-1} (Table 5).

The d_π-π conjugation effect between the Pt center and the chelated phenyl ring will increase the electron density on –POPh in ligand **L-P** to make it more difficult to be reduced. So, **P-Pt-N** shows a lower E_{pc} (-2.24 V) than **N-Pt-P** (-2.03 V). However, this kind of conjugation effect makes the –NPh_2 unit in the ligand **L-N** easier to be oxidized. As a result, **P-Pt-N** shows a higher E_{pa} (0.40 V) than **N-Pt-P** (0.36 V). Hence, the **P-Pt-N** should exhibit lower injection ability for both kinds of charge carriers than **N-Pt-P**. On the other hand, as indicated by the results of the hole-only devices for **S-Pt-N** and **N-Pt-P** (Figure 16), it seems that the –NPh_2 moiety on the ligand **L-N** should be more effective in conferring hole-transporting ability to the concerned Pt^{II} complexes with respect to that of the N-donating ligand. So, **P-Pt-N** should show lower hole injection/transporting ability than **N-Pt-P**. Besides, the AIE nature endows **N-Pt-P** with higher Φ_p than **P-Pt-N** in PMMA film (Table 1). As a result, compared with device **A2** fabricated by **N-Pt-P**, device **C2** based on **P-Pt-N** displays

lower EL efficiencies with L_{max} of 15163cd m^{-2}, η_{ext} of 21.7%, η_L of 57.4 cd A^{-1} and η_P of 44.7 lm W^{-1} (Table 5).

Generally, these Pt^{II} complexes achieve enhanced charge carrier injection/transporting abilities from the $–NPh_2$, $–SO_2Ph$ and $–POPh_2$ functional moieties. Together with the AIE nature, these Pt^{II} complexes even outperform previously reported EL performance with respect to that of traditional Pt^{II}(C^N)acac complexes bearing $–NPh_2$, $–SO_2Ph$ and $–POPh_2$ moieties.[7, 18] To date, enormous excellent research on OLEDs with AIE fluorescent emitters with good EL performances have been reported.[28, 68-70] However, researches on AIE phosphorescence OLEDs are still rare. Recently, Li *et al* reported two AIE-active Ir^{III} complexes and their solution-processed devices can show a η_{ext} of 7.6% and η_L of 25.7 cd A^{-1}.[71] Zheng *et al* built a green-blue OLED from the AIE-active Ir(III) complex bearing *tetra*-phenylimidodiphosphinate ligand, achieving high EL efficiency of 67.95 cd A^{-1}.[72] The η_{ext} of 0.35% has been achieved by incorporating an AIE-Active mono-cyclometalated Ir^{III} complex into supramolecular branched wires.[73] Two AIE-active Pt^{II} complexes with a EL efficiencies of 18.4 cd A^{-1} and 5.8% have been reported by Yam's group.[35] Hiroto Fukuda *et al*. reported a emitter using Pt(topy)(Htopy)Cl complex and its analogs showing η_L of 0.5 cd A^{-1}, η_P of 0.2 lm W^{-1} and η_{ext} of 0.2%, but their AIE feature has not been explicited.[41] Compared with these reported results, the EL efficiencies of the presented AIE-active Pt^{II}(C^N)(N-donor ligand)Cl complexes are higher, and they are advantageous, indicating their promising prospect in the EL application. This investigation definitely furnishes a new possibility for exploring novel Pt^{II} complexes with AIE nature and achieving high EL efficiency.

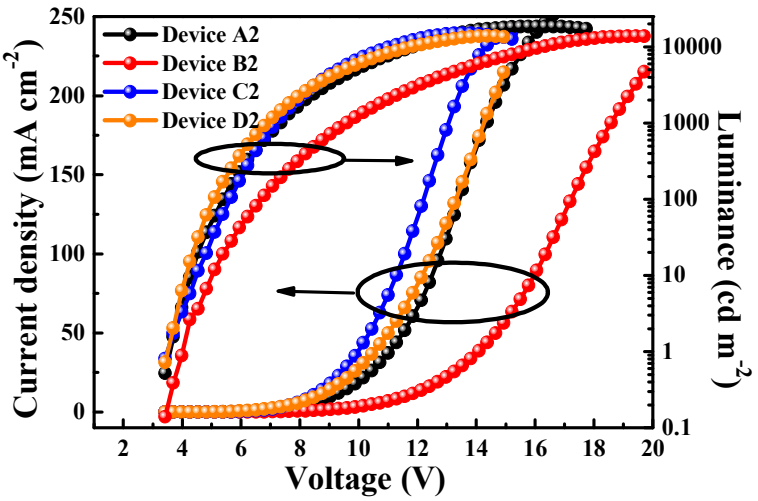

Figure 14. Current density–voltage–luminance (*J*–*V*–*L*) relationships of the optimized devices

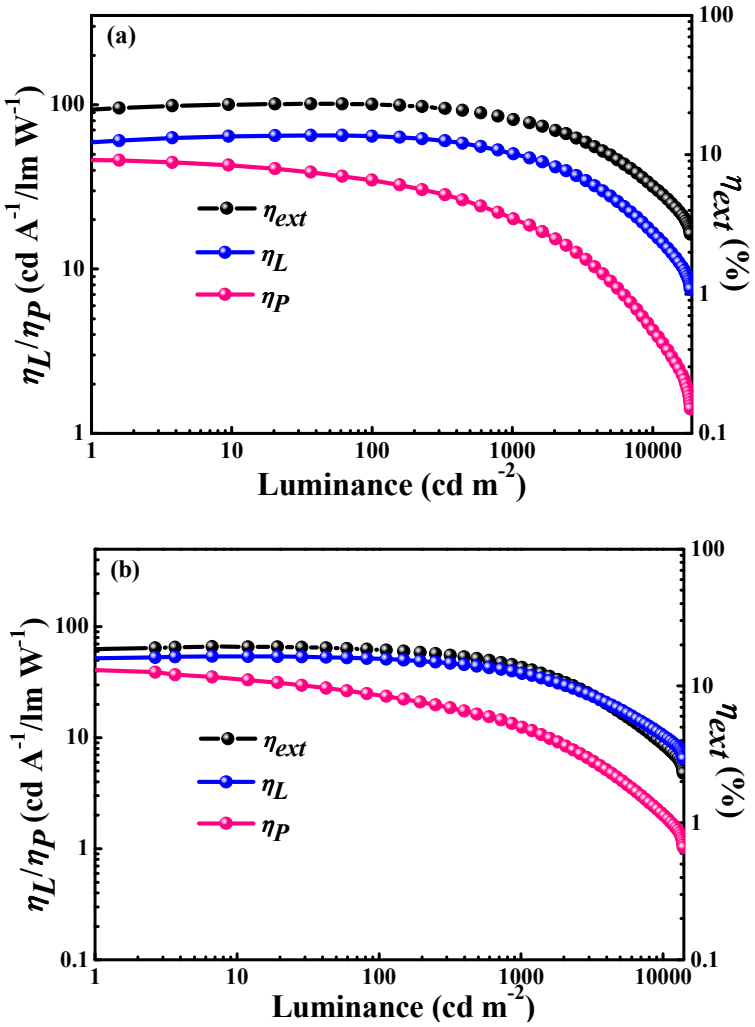

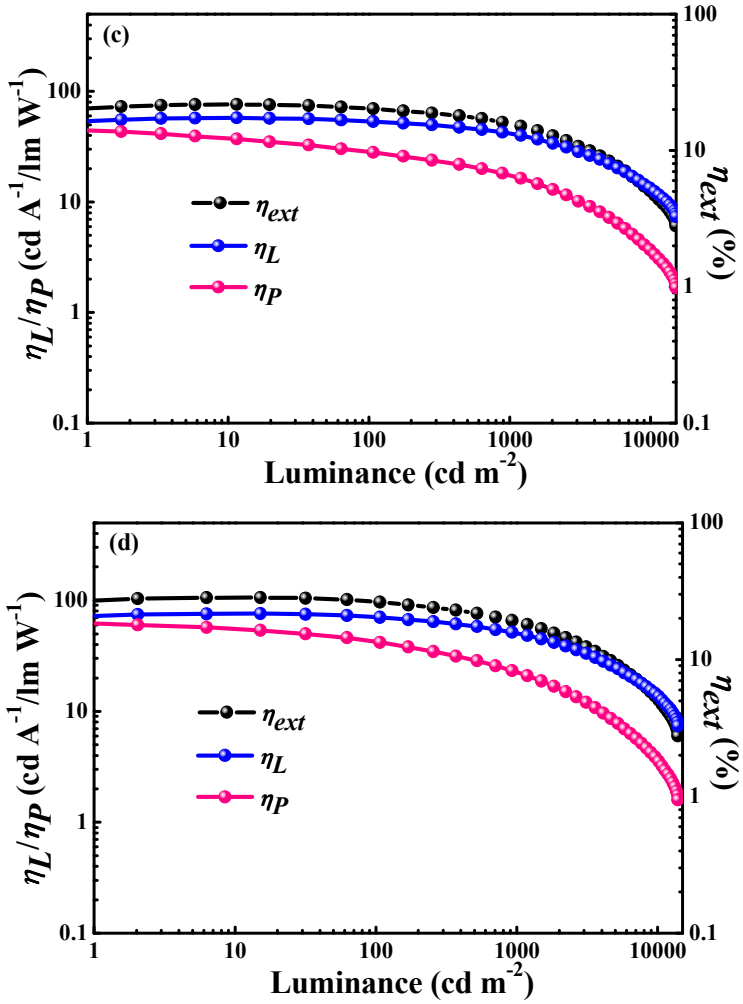

Figure 15. EL efficiency–luminance curves for the optimized devices. (a) Device **A2**, (b) Device **B2**, (c) Device **C2** and (d) Device **D2**

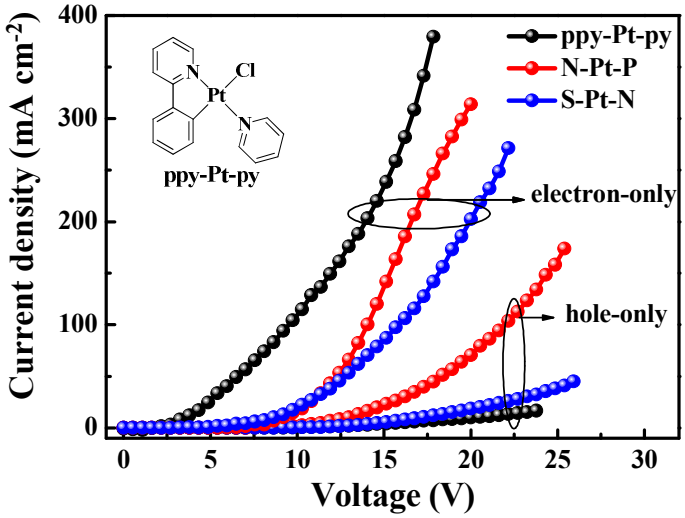

Figure 16. Current density−voltage (*J-V*) curves for single carrier devices with neat film using **N-Pt-P** and **S-Pt-N** as active layer, and their parent complex **ppy-Pt-py** as reference. Hole-only

device: ITO/MoO_3 (3nm)/PEDOT: PSS (20 nm)/active layer (50 nm)/NPB (30nm)/MoO_3 (3 nm)/Al (100 nm); electron-only device: ITO/LiF (3nm)/active layer (50 nm)/LiF (3 nm)/Al (100 nm)

Conclusion

In summary, four AIE-active Pt^{II}(C^N)(N-donor ligand)Cl complexes have been successfully developed and their structures are verified by NMR, MS and X-ray crystallography characterization. Their photophysical behavior has been clarified by theoretical calculations. These Pt^{II} complexes exhibit weak phosphorescent emission in solution, but very strong phosphorescence in PMMA films with a maximal Φ_p of 72.0%, which is much higher than that in solution. The outstanding AIE nature of these Pt^{II} complexes should be in favor of enhancing their EL performance. The $–SO_2Ph$ and $–POPh_2$ moieties with EI/ET ability and $–NPh_2$ moiety showing HI/HT property endow the complexes with balanced charge carrier injection/transporting abilities in accordance to the single carrier device results. Consequently, their solution-processed OLEDs display highly efficient EL efficiencies with a maximal external η_{ext} of 28.4%, a maximal η_L of 75.9 cd A^{-1} and a maximal η_P of 62.7 lm W^{-1}, representing the top-ranking EL performances ever achieved by AIE-active phosphorescent complexes. To the best of our knowledge, studies on Pt^{II} complexes with AIE feature are very limited. Hence, these AIE-active Pt^{II}(C^N)(N-donor ligand)Cl emitters should be rare examples in EL application, herein providing useful information for exploring AIE-active Pt^{II} complexes with high EL ability.

ASSOCIATED CONTENT

Supporting Information

Synthesis of borate compounds **B-S** and **B-P**, NMR and MS spectra of these Pt^{II} complexes, TGA,

DSC and CV curves, DLS results, Single crystal data of **S-Pt-N**, some PL spectra of these Pt^{II} complexes and EL data.

This material is available free of charge via the Internet at http://pubs.acs.org.

Author Contributions

J.Z. prepared all the complexes and characterized both the basic photophysical and EL properties. Z.F. and D.K.Z. prepared some intermediate compounds. Y.W. did the theoretical calculations. X.L.Y. measured the CV curves. Z.X.W. designed the structure of the OLEDs. G.J.Z. designed the complexes and supervised the overall project. G.J.Z. also contributed to analysis of all the data.

AUTHOR INFORMATION

Corresponding Authors

*E-mail: zhougj@mail.xjtu.edu.cn. (G.J.Z.)

*E-mail: zhaoxinwu@mail.xjtu.edu.cn. (Z.X.W.)

ORCID

Guijiang Zhou: 0000-0002-5863-3551

Zhaoxin Wu: 0000-0003-2979-3051

Notes

The authors declare no competing financial interest.

Acknowledgement

We thank the National Natural Science Foundation of China (No. 21572176, 21602170 and 20902072), the Fundamental Research Funds for the Central Universities (cxtd2015003 and

01091191320074), the China Postdoctoral Science Foundation (Grant no. 20130201110034, 2014M562403) and the Key Creative Scientific Research Team in Yulin City of Shaanxi Province.

References

(1) Tang, C. W.; VanSlyke, S. A., Organic electroluminescent diodes. *Appl. Phys. Lett.* **1987**, *51*, 913-915.

(2) Baldo, M.; Thompson, M.; Forrest, S., High-efficiency fluorescent organic light-emitting devices using a phosphorescent sensitizer. *Nature* **2000**, *403*, 750-753.

(3) Baldo, M. A.; O'brien, D.; You, Y.; Shoustikov, A.; Sibley, S.; Thompson, M.; Forrest, S., Highly efficient phosphorescent emission from organic electroluminescent devices. *Nature* **1998**, *395*, 151-154.

(4) D'Andrade, B. W.; Forrest, S. R., White organic light-emitting devices for solid-state lighting. *Adv. Mater.* **2004**, *16*, 1585-1595.

(5) Kalinowski, J.; Fattori, V.; Cocchi, M.; Williams, J. A. G., Light-emitting devices based on organometallic platinum complexes as emitters. *Coord. Chem. Rev.* **2011**, *255*, 2401-2425.

(6) Yang, X.; Yao, C.; Zhou, G., Highly Efficient Phosphorescent Materials Based on Platinum Complexes and Their Application in Organic Light-Emitting Devices (OLEDs). *Platinum Met. Rev.* **2013**, *57*, 2-16.

(7) Zhou, G.; Wang, Q.; Wang, X.; Ho, C.-L.; Wong, W.-Y.; Ma, D.; Wang, L.; Lin, Z., Metallophosphors of platinum with distinct main-group elements: a versatile approach towards color tuning and white-light emission with superior efficiency/color quality/brightness trade-offs. *J. Mater. Chem.* **2010**, *20*, 7472-7484.

(8) Fan, C.; Yang, C., Yellow/orange emissive heavy-metal complexes as phosphors in monochromatic and white organic light-emitting devices. *Chem. Soc. Rev.* **2014**, *43*, 6439-6469.

(9) Yam, V. W.-W.; Au, V. K.-M.; Leung, S. Y.-L., Light-Emitting Self-Assembled Materials Based on d8 and d10 Transition Metal Complexes. *Chem. Rev.* **2015**, *115*, 7589-7728.

(10) Baldo, M.; O'brien, D.; Thompson, M.; Forrest, S., Excitonic singlet-triplet ratio in a semiconducting organic thin film. *Phys. Rev. B* **1999**, *60*, 14422.

(11) Yersin, H.; Rausch, A. F.; Czerwieniec, R.; Hofbeck, T.; Fischer, T., The triplet state of organo-transition metal compounds. Triplet harvesting and singlet harvesting for efficient OLEDs. *Coord. Chem. Rev.* **2011**, *255*, 2622-2652.

(12) Chen, Y.; Li, K.; Lu, W.; Chui, S. S.; Ma, C. W.; Che, C. M., Photoresponsive Supramolecular Organometallic Nanosheets Induced by Pt···Pt and CH···π Interactions. *Angew. Chem. Int. Ed.* **2009**, *48*, 9909-9913.

(13) Kui, S. C. F.; Hung, F.-F.; Lai, S.-L.; Yuen, M.-Y.; Kwok, C.-C.; Low, K.-H.; Chui, S. S.-Y.; Che, C.-M., Luminescent Organoplatinum(II) Complexes with Functionalized Cyclometalated C^N^C Ligands: Structures, Photophysical Properties, and Material Applications. *Chem. Eur. J.* **2012**, *18*, 96-109.

(14) Lu, W.; Mi, B.-X.; Chan, M. C.; Hui, Z.; Che, C.-M.; Zhu, N.; Lee, S.-T., Light-emitting tridentate cyclometalated platinum (II) complexes containing σ-alkynyl auxiliaries: tuning of

photo-and electrophosphorescence. *J. Am. Chem. Soc.* **2004**, *126*, 4958-4971.
(15) Ravindranathan, D.; Vezzu, D. A.; Bartolotti, L.; Boyle, P. D.; Huo, S., Improvement in phosphorescence efficiency through tuning of coordination geometry of tridentate cyclometalated platinum (II) complexes. *Inorg. Chem.* **2010**, *49*, 8922-8928.
(16) Chepelin, O.; Ujma, J.; Barran, P. E.; Lusby, P. J., Sequential, Kinetically Controlled Synthesis of Multicomponent Stereoisomeric Assemblies. *Angew. Chem. Int. Ed.* **2012**, *51*, 4194-4197.
(17) Xu, X.; Zhao, Y.; Dang, J.; Yang, X.; Zhou, G.; Ma, D.; Wang, L.; Wong, W. Y.; Wu, Z.; Zhao, X., Simple tuning of the optoelectronic properties of Ir^{III} and Pt^{II} electrophosphors based on linkage isomer formation with a naphthylthiazolyl moiety. *Eur. J. Inorg. Chem.* **2012**, *2012*, 2278-2288.
(18) Yang, X.; Xu, X.; Zhao, J.; Dang, J.-S.; Huang, Z.; Yan, X.; Zhou, G.; Wang, D., Phosphorescent Platinum (II) Complexes Bearing 2-Vinylpyridine-type Ligands: Synthesis, Electrochemical and Photophysical Properties, and Tuning of Electrophosphorescent Behavior by Main-Group Moieties. *Inorg. Chem.* **2014**, *53*, 12986-13000.
(19) Xu, H.; Chen, R.; Sun, Q.; Lai, W.; Su, Q.; Huang, W.; Liu, X., Recent progress in metal-organic complexes for optoelectronic applications. *Chem. Soc. Rev.* **2014**, *43*, 3259-302.
(20) Huang, C. H.; Li, F.; Huang, W., Introduction to Organic Light-Emitting Materials and Devices. *Press of Fudan University, Shanghai* **2005**.
(21) Komiya, N.; Muraoka, T.; Iida, M.; Miyanaga, M.; Takahashi, K.; Naota, T., Ultrasound-induced emission enhancement based on structure-dependent homo- and heterochiral aggregations of chiral binuclear platinum complexes. *J. Am. Chem. Soc.* **2011**, *133*, 16054-61.
(22) D'Andrade, B. W.; Brooks, J.; Adamovich, V.; Thompson, M. E.; Forrest, S. R., White Light Emission Using Triplet Excimers in Electrophosphorescent Organic Light-Emitting Devices. *Adv. Mater.* **2002**, *14*, 1032-1036.
(23) Luo, J.; Xie, Z.; Lam, J. W.; Cheng, L.; Chen, H.; Qiu, C.; Kwok, H. S.; Zhan, X.; Liu, Y.; Zhu, D.; Tang, B. Z., Aggregation-induced emission of 1-methyl-1, 2, 3, 4, 5-pentaphenylsilole. *Chem. Commun.* **2001**, 1740-1741.
(24) Hong, Y.; Lam, J. W.; Tang, B. Z., Aggregation-induced emission. *Chem. Soc. Rev.* **2011**, *40*, 5361-5388.
(25) Mei, J.; Leung, N. L.; Kwok, R. T.; Lam, J. W.; Tang, B. Z., Aggregation-Induced Emission: Together We Shine, United We Soar! *Chem. Rev.* **2015**, *115*, 11718-11940.
(26) Pasha, S.; Alam, P.; Dash, S.; Kaur, G.; Banerjee, D.; Chowdhury, R.; Rath, N.; Roychoudhury, A.; Laskar, I., Rare observation of `aggregation induced emission' in cyclometalated platinum(II) complexes and their biological activities. *RSC Adv.* **2014**, *4*, 50549-50553.
(27) Pasha, S. S.; Alam, P.; Sarmah, A.; Roy, R. K.; Laskar, I. R., Encapsulation of multi-stimuli AIE active platinum(II) complex: a facile and dry approach for luminescent mesoporous silica. *RSC Adv.* **2016**, 87791-87795.
(28) Yuan, W. Z.; Gong, Y.; Chen, S.; Shen, X. Y.; Lam, J. W. Y.; Lu, P.; Lu, Y.; Wang, Z.; Hu, R.; Xie, N.; Kwok, H. S.; Zhang, Y.; Sun, J. Z.; Tang, B. Z., Efficient Solid Emitters with Aggregation-Induced Emission and Intramolecular Charge Transfer Characteristics: Molecular Design, Synthesis, Photophysical Behaviors, and OLED Application. *Chem. Mater.* **2012**, *24*, 1518-1528.
(29) Ravotto, L.; Ceroni, P., Aggregation induced phosphorescence of metal complexes: From principles to applications. *Coord. Chem. Rev.* **2017**, *346*, 62-76.
(30) Honda, H.; Kuwabara, J.; Kanbara, T., Aggregation-induced emission behavior of a pincer

platinum(II) complex bearing a poly(ethylene oxide) chain in aqueous solution. *J. Organomet. Chem.* **2014**, *772-773*, 139-142.
(31) Zhu, M.-X.; Lu, W.; Zhu, N.; Che, C.-M., Structures and Solvatochromic Phosphorescence of Dicationic Terpyridyl–Platinum(II) Complexes with Foldable Oligo(ortho-phenyleneethynylene) Bridging Ligands. *Chem. Eur. J.* **2008**, *14*, 9736-9746.
(32) Sathish, V.; Ramdass, A.; Thanasekaran, P.; Lu, K. L.; Rajagopal, S., Aggregation-induced phosphorescence enhancement (AIPE) based on transition metal complexes—An overview. *J Photochem Photobiol C* **2015**, *23*, 25-44.
(33) Liu, S.; Sun, H.; Ma, Y.; Ye, S.; Liu, X.; Zhou, X.; Mou, X.; Wang, L.; Zhao, Q.; Huang, W., Rational design of metallophosphors with tunable aggregation-induced phosphorescent emission and their promising applications in time-resolved luminescence assay and targeted luminescence imaging of cancer cells. *J. Mater. Chem.* **2012**, *22*, 22167-22173.
(34) Liu, R.; Zhu, S.; Lu, J.; Shi, H.; Zhu, H., Pt(II) diimine complexes bearing difluoro-boron-dipyrromethene acetylide ligands: Synthesis, photophysics, aggregation included emission and optical power limiting properties. *Dyes & Pigments* **2017**, *147*, 291-299.
(35) Li, Y.; Tsang, D. P.-K.; Chan, C. K.-M.; Wong, K. M.-C.; Chan, M.-Y.; Yam, V. W.-W., Synthesis of Unsymmetric Bipyridine–PtII–Alkynyl Complexes through Post-Click Reaction with Emission Enhancement Characteristics and Their Applications as Phosphorescent Organic Light-Emitting Diodes. *Chem. Eur. J.* **2014**, *20*, 13710-13715.
(36) Cho, J. Y.; Suponitsky, K. Y.; Li, J.; Timofeeva, T. V.; Barlow, S.; Marder, S. R., Cyclometalated platinum complexes: High-yield synthesis, characterization, and a crystal structure. *J. Organomet. Chem.* **2005**, *690*, 4090-4093.
(37) Tomoko, O.; El-Mehasseb, I. M.; Kodaka, M.; Tomohiro, T.; Okamoto, K.-i.; Okuno, H., Mononuclear Platinum(II) Complex with 2-Phenylpyridine Ligands Showing High Cytotoxicity against Mouse Sarcoma 180 Cells Acquiring High Cisplatin Resistance. *J. Med. Chem.* **2001**, *44*, 4661.
(38) Edwards, G. L.; Black, D. S. C.; Deacon, G. B.; Wakelin, L. P., In vitro and in vivo studies of neutral cyclometallated complexes against murine leukæmias. *Can. J. Chem.* **2005**, *83*, 980-989(10).
(39) Yoon, M.-S.; Ryu, D.-W.; Kim, J.-R.; Ramesh, R.; Ahn, K.-H., Cyclometalated platinum (II) complexes derived from a chiral pyridine ligand: Synthesis, structure, and catalytic activity. *Bull. Korean Chem. Soc.* **2007**, *28*, 2045-2050.
(40) Zhao, J.; Dang, F.; Feng, Z.; Liu, B.; Yang, X.; Wu, Y.; Zhou, G.; Wu, Z.; Wong, W.-Y., Highly efficient electroluminescent PtII ppy-type complexes with monodentate ligands. *Chem. Commun.* **2017**, *53*, 7581-7584.
(41) Fukuda, H.; Yamada, Y.; Hashizume, D.; Takayama, T.; Watabe, M., [Pt(topy)(Htopy)(ONO2)] complex (Htopy = 2-p-tolylpyridine) and its analogs: 195Pt NMR spectra and fabrication of light-emitting devices. *Appl. Organomet. Chem.* **2009**, *23*, 154-160.
(42) Wong, W.-Y.; Ho, C.-L., Functional metallophosphors for effective charge carrier injection/transport: new robust OLED materials with emerging applications. *J. Mater. Chem.* **2009**, *19*, 4457-4482.
(43) Lu, G. Z.; Jing, Y. M.; Han, H. B.; Fang, Y. L.; Zheng, Y. X., Efficient Electroluminescence of Two Heteroleptic Platinum Complexes with a 2-(5-Phenyl-1,3,4-oxadiazol-2-yl)phenol Ancillary Ligand. *Organometallics* **2016**, *35*, 448-454.
(44) Yang, X.; Zhou, G.; Wong, W. Y., Functionalization of phosphorescent emitters and their host

materials by main-group elements for phosphorescent organic light-emitting devices. *Chem. Soc. Rev.* **2015**, *44*, 8484-575.

(45) Xu, X.; Guo, H.; Zhao, J.; Liu, B.; Yang, X.; Zhou, G.; Wu, Z., Asymmetric tris-Heteroleptic Iridium^{III} Complexes Containing 9-phenyl-9-phosphafluorene Oxide Moiety with Enhanced Charge Carrier Injection/Transporting Properties for Highly Efficient Solution-Processed Organic Light-Emitting Diodes (OLEDs). *Chem. Mater.* **2016**, *28*, 8556-8569.

(46) Xu, X.; Yang, X.; Dang, J.; Zhou, G.; Wu, Y.; Li, H.; Wong, W. Y., Trifunctional Ir(III) ppy-type asymmetric phosphorescent emitters with ambipolar features for highly efficient electroluminescent devices. *Chem. Commun.* **2014**, *50*, 2473-2476.

(47) Zhou, G.; Ho, C. L.; Wong, W. Y.; Wang, Q.; Ma, D.; Wang, L.; Lin, Z.; Marder, T. B.; Beeby, A., Manipulating Charge-Transfer Character with Electron-Withdrawing Main-Group Moieties for the Color Tuning of Iridium Electrophosphors. *Adv. Funct. Mater.* **2008**, *18*, 499-511.

(48) Esmaeilbeig, A.; Samouei, H.; Abedanzadeh, S.; Amirghofran, Z., Synthesis, characterization and antitumor activity study of some cyclometalated organoplatinum(II) complexes containing aromatic N-donor ligands. *J. Organomet. Chem.* **2011**, *696*, 3135-3142.

(49) Lai, S. W.; Chan, M. C. W.; Cheung, K. K.; Shieming Peng, A.; Che, C. M., Synthesis of Organoplatinum Oligomers by Employing N-Donor Bridges with Predesigned Geometry: Structural and Photophysical Properties of Luminescent Cyclometalated Platinum(II) Macrocycles. *Organometallics* **1999**, *18*, 3991-3997.

(50) Hofbeck, T.; Yersin, H., The Triplet State of *fac*-Ir(ppy)$_3$. *Inorg. Chem.* **2010**, *49*, 9290-9299.

(51) Mdleleni, M. M.; Bridgewater, J. S.; Watts, R. J.; Ford, P. C., Synthesis, Structure, and Spectroscopic Properties of Ortho-Metalated Platinum(II) Complexes. *Inorg. Chem.* **1995**, *34*, 2334-2342.

(52) Ghavale, N.; Wadawale, A.; Dey, S.; Jain, V. K., Synthesis, structures and spectroscopic properties of platinum complexes containing orthometalated 2-phenylpyridine. *J. Organomet. Chem.* **2010**, *695*, 1237-1245.

(53) Stacey, O. J.; Platts, J. A.; Coles, S. J.; Horton, P. N.; Pope, S. J. A., Phosphorescent, Cyclometalated Cinchophen-Derived Platinum Complexes: Syntheses, Structures, and Electronic Properties. *Inorg. Chem.* **2015**, *54*, 6528-6536.

(54) Aldridge, T. K.; Stacy, E. M.; McMillin, D. R., Studies of the Room-Temperature Absorption and Emission Spectra of [Pt(trpy)X]$^+$ Systems. *Inorg. Chem.* **1994**, *33*, 722-727.

(55) Bailey, J. A.; Hill, M. G.; Marsh, R. E.; Miskowski, V. M.; Schaefer, W. P.; Gray, H. B., Electronic Spectroscopy of Chloro(terpyridine)platinum(II). *Inorg. Chem.* **1995**, *34*, 4591-4599.

(56) Williams, J. A. G., Photochemistry and Photophysics of Coordination Compounds: Platinum. *Top Curr Chem* **2007**, *281*, 205-268.

(57) Michalec, J. F.; Bejune, S. A.; Cuttell, D. G.; Summerton, G. C.; Gertenbach, J. A.; Field, J. S.; Haines, R. J.; McMillin, D. R., Long-Lived Emissions from 4‘-Substituted Pt(trpy)Cl$^+$ Complexes Bearing Aryl Groups. Influence of Orbital Parentage. *Inorg. Chem.* **2001**, *40*, 2193-2200.

(58) Rausch, A. F.; Homeier, H.; Djurovich, P. I.; Thompson, M. E.; Yersin, H. Spin-orbit coupling routes and OLED performance: studies of blue-light emitting Ir(III) and Pt(II) complexes, *Proc. SPIE* **2007**, *6655*, 66550F: 1-16.

(59) Xun, Z.; Tang, H.; Zeng, Y.; Chen, J.; Yu, T.; Zhang, X.; Li, Y., Synthesis and Aggregation-induced Emission of Tetraphenylethylene Derivatives Based on Hexakisphenylbenzene Backbone. *Acta Chim. Sinica* **2015**, *73*, 819-825.

(60) Tong, H.; Hong, Y.; Dong, Y.; Häussler, M.; Li, Z.; Lam, J. W. Y.; Dong, Y.; Sung, H. H. Y.; Williams, I. D.; Tang, B. Z., Protein Detection and Quantitation by Tetraphenylethene-Based Fluorescent Probes with Aggregation-Induced Emission Characteristics. *J Phys Chem B* **2007**, *111*, 11817-11823.

(61) Honda, H.; Ogawa, Y.; Kuwabara, J.; Kanbara, T., Emission Behavior of Secondary Thioamide-Based Cationic Pincer Platinum(II) Complexes in the Aggregate State. *Eur. J. Inorg. Chem.* **2014**, *2014*, 1865-1869.

(62) Mei, J.; Hong, Y.; Lam, J. W. Y.; Qin, A.; Tang, Y.; Tang, B. Z., Aggregation-Induced Emission: The Whole Is More Brilliant than the Parts. *Adv. Mater.* **2014**, *26*, 5429-5479.

(63) Li, Z.; Wu, Z.; Fu, W.; Liu, P.; Jiao, B.; Wang, D.; Zhou, G.; Hou, X., Versatile fluorinated derivatives of triphenylamine as hole-transporters and blue-violet emitters in organic light-emitting devices. *J. Phys. Chem. C* **2012**, *116*, 20504-20512.

(64) Zhou, G.; Wong, W. Y.; Yao, B.; Xie, Z.; Wang, L., Triphenylamine-Dendronized Pure Red Iridium Phosphors with Superior OLED Efficiency/Color Purity Trade-Offs. *Angew. Chem. Int. Ed.* **2007**, *46*, 1149-1151.

(65) Balashev, K. P.; Puzyk, M. V.; Kotlyar, V. S.; Kulikova, M. V., Photophysics, photochemistry and electrochemistry of mixed-ligand platinum (II) complexes with 2-phenylpyridine and 2-(2′-thienyl) pyridine as cyclometalating ligands. *Coord. Chem. Rev.* **1997**, *159*, 109-120.

(66) Kvam, P.-I.; Puzyk, M.; Balashev, K. P.; Songstad, J., Spectroscopic and electrochemical properties of some mixed-ligand cyclometalated platinum (II) complexes derived from 2-phenylpyridine. *Acta Chem. Scand.* **1995**, *49*, 335-343.

(67) Zhao, J.; Yu, Y.; Yang, X.; Yan, X.; Zhang, H.; Xu, X.; Zhou, G.; Wu, Z.; Ren, Y.; Wong, W. Y., Phosphorescent Iridium(III) Complexes Bearing Fluorinated Aromatic Sulfonyl Group with Nearly Unity Phosphorescent Quantum Yields and Outstanding Electroluminescent Properties. *ACS Appl. Mater. Interfaces* **2015**, *7*, 24703-24714.

(68) Vyas, V. S.; Rathore, R., Preparation of a tetraphenylethylene-based emitter: synthesis, structure and optoelectronic properties of tetrakis(pentaphenylphenyl)ethylene. *Chem. Commun.* **2010**, *46*, 1065-1067.

(69) Zhao, Z.; Chen, S.; Lam, J. W.; Lu, P.; Zhong, Y.; Wong, K. S.; Kwok, H. S.; Tang, B. Z., Creation of highly efficient solid emitter by decorating pyrene core with AIE-active tetraphenylethene peripheries. *Chem. Commun.* **2010**, *46*, 2221-2223.

(70) Zhao, Z.; Jacky, W. Y. L.; Tang, B. Z., Aggregation-Induced Emission of Tetraarylethene Luminogens. *Curr. Org. Chem.* **2010**, *14*, 2109-2132.

(71) Li, P.; Zeng, Q.-Y.; Sun, H.-Z.; Akhtar, M.; Shan, G.-G.; Hou, X.-G.; Li, F.-S.; Su, Z.-M., Aggregation-induced emission (AIE) active iridium complexes toward highly efficient single-layer non-doped electroluminescent devices. *J. Mater. Chem. C* **2016**, *4*, 10464-10470.

(72) Zhu, Y. C.; Zhou, L.; Li, H. Y.; Xu, Q. L.; Teng, M. Y.; Zheng, Y. X.; Zuo, J. L.; Zhang, H. J.; You, X. Z., Highly efficient green and blue-green phosphorescent OLEDs based on iridium complexes with the tetraphenylimidodiphosphinate ligand. *Adv. Mater.* **2011**, *23*, 4041-4046.

(73) Maji, S.; Alam, P.; Kumar, G. S.; Biswas, S.; Sarkar, P. K.; Das, B.; Rehman, I.; Das, B. B.; Jana, N. R.; Laskar, I. R., Induced Aggregation of AIE-Active Mono-Cyclometalated Ir(III) Complex into Supramolecular Branched Wires for Light-Emitting Diodes. *Small* **2017**, *13*, 1603780.

Table of content